THESIS FOR THE DEGREE OF DOCTOR OF PHILOSOPHY

Microstructure Evolution and Mechanical Properties

of

Haynes 282

CEENA JOSEPH

Department of Industrial and Materials Science
CHALMERS UNIVERSITY OF TECHNOLOGY
Göteborg, Sweden, 2018

Microstructure Evolution and Mechanical Properties of Haynes 282

CEENA JOSEPH
ISBN:978-91-7597-701-0

Doktorsavhandlingar vid Chalmers tekniska högskola
Ny serie nr 4382
ISSN 0346-718X

Department of Industrial and Materials Science
Chalmers University of Technology
SE-412 96 Göteborg
Sweden
Tel:+46 (0)31 772 1000

Printed by Chalmers Reproservice
Göteborg, Sweden 2018

Dedication

To

My Daughters

Adina  & Alina 

Microstructure Evolution and Mechanical Properties of Haynes 282

CEENA JOSEPH
Department of Industrial and Materials Science
Chalmers University of Technology

Abstract

Precipitation-hardened nickel-based superalloys find wide applications in aero engines and land-based gas turbines due to a combination of properties such as high temperature strength, resistance to oxidation and corrosion, fabricability, and creep strength. Structural engine components are traditionally cast to achieve higher degree of geometrical design freedom. However, the latest fabrication strategy to achieve low cost and light weight structural components is by joining materials based on temperature needs. The challenge in this strategy is to tailor the heat treatment to suit the multi-material structures and still be able to meet the desired property requirements. This requires a profound understanding of the process-structure-property relationships in these complex alloys. The newly introduced Ni-base superalloy Haynes 282 has been attracting interest due to its high-temperature properties and excellent weldability. These properties are achieved due to the precipitation of strengthening phase (γ′, Ni_3 (Al,Ti)) and grain boundary carbides (mainly $M_{23}C_6$ and M_6C) during heat treatment.

As Haynes 282 has showed sensitivity to heat treatment temperatures within the typical tolerance limits around the conventional heat treatment, the main objective of this research was to understand the microstructural evolution and mechanical properties with changes in heat treatment conditions. The effect of heat treatment variations on microstructure and mechanical properties has been systematically studied. Its influence on microstructure and tensile properties between room temperature and 730 °C are presented.

The results show that γ′ does not precipitate during rapid cooling but it precipitates as fine spherical particles during air cooling from the carbide stabilization temperature, and it changes to bimodal distribution with square and spherical morphology during slow cooling. During ageing, γ′ is seen to precipitate intergranularly, as well as along the grain boundaries. The solvus temperature for this phase was above 1010 °C (higher than previously suggested), and depending on the combination of temperatures and times of the heat treatments, the γ′ morphology changes from spherical to bi-modal to cuboidal. The grain boundary carbide morphology depends strongly on heat treatment temperature and is seen to change from continuous film to brick wall structure and finally to discrete particles. These microstructural changes strongly affect both strength and ductility of the material.

Furthermore, Haynes 282 forgings show ductility variations in short transverse direction. The lower limit of ductility in this direction is close to the design tolerance and thus creates a need

to understand the underlying cause. In this part, the study is focused to understand ductility variation by microscopic investigations. Carbide segregation and banding is seen to influence the ductility when oriented perpendicular to the tensile axis. This influence is also qualitatively captured through micromechanical modelling.

Keywords: Haynes 282, gamma prime, carbides, isothermal transformation, anisotropy ductility, heat treatment, microstructure, solution treatment, carbide stabilization treatment

Preface

This licentiate thesis is based on the work performed at the Department of Industrial Materials Science (Previous Materials and Manufacturing Technology), Chalmers University of Technology during the period June 2012-Dec 2017. During this period the work was performed within the project funded by Swedish National Aeronautical Research Program (NFFP6) under the supervision of Professor Christer Persson and Docent Magnus Hörnqvist Colliander.

This thesis consists of an introductory part followed by the appended papers.

List of Appended papers

Paper I: **Anisotropy of room temperature Ductility in Haynes 282 forgings**

C. Joseph, M. Hörnqvist Colliander, C. Persson

Proceedings of the 8th International Symposium on Superalloy 718 and Derivatives, p. 601-609

Paper II: **Influence of Carbide distribution on Ductility of Haynes 282 forgings**

C. Joseph, M. Hörnqvist Colliander, R. Brommesson, C. Persson

13th International Symposium on Superalloys, SUPERALLOYS 2016, Seven Springs Mountain Resort Seven Springs, United States, 11 September 2016 through 15 September 2016, p. 523-529

Paper III: **Influence of Heat treatments on the Microstructure and Tensile Properties of Haynes 282 sheet material**

C. Joseph, C. Persson, M. Hörnqvist Colliander

Materials Science & Engineering A: Structural Materials: Properties, Microstructure and Processing. Vol. 679, p. 520-530

https://doi.org/10.1016/j.msea.2016.10.048

Paper IV: **Gamma prime Precipitation in a Nickel base Superalloy during cooling**

C. Joseph, M. Thuvander , J. Moverare , C. Persson and M. Hörnqvist Colliander

Submitted for journal publication

Paper V: **Isothermal Phase Transformation in Nickel base Superalloy Haynes 282**

C. Joseph, C. Persson and M. Hörnqvist Colliander

Submitted for journal publication

Paper VI: **Microstructure and Mechanical Properties of Haynes 282 - Effect of variations in Solution Treatment**

C. Joseph, S Sreekanth, B. Pettersson, C. Persson, M. Hörnqvist Colliander

In Manuscript

Paper VII: **Effect of Variations in Carbide Stabilization Treatment on Microstructure and Mechanical properties of Haynes 282**

C. Joseph, M. Hörnqvist Colliander, B. Pettersson, C. Persson

In Manuscript

Paper not appended to the thesis

Paper I: **Dynamic strain aging in Haynes 282 superalloy**

M. Hörnqvist Colliander, C. Joseph, C. Persson et al

Proceedings of the 2nd Euro Superalloys Conference. Vol. 14, p. Art. no. 16002-

Paper II: **3D grain structure modelling of intergranular fracture in forged Haynes 282**

R. Brommesson, M. Ekh, C. Joseph

Engineering Fracture Mechanics. Vol. 154, p. 57-71

https://doi.org/10.1016/j.engfracmech.2015.12.030

Contribution to the appended papers

My contribution to the appended papers is as follows

Paper I: The work was planned together with GKN aerospace. I did the microscopy work and wrote the paper in cooperation with the co-authors.

Paper II: The work was planned together with GKN aerospace. I did the microscopy work and the modelling part was done by Rebecka Brommesson. The paper was written by me with in cooperation with the co-authors.

Paper III: The work was planned by me in collaboration with my supervisors. The experimental work was performed by me. Mechanical testing was done by Prof. Christer Persson. The paper was written by me in cooperation with the co-authors.

Paper IV: The work was planned by me in collaboration with my supervisors. The preparation of the APT specimens was done by me with help from Dr.Mattias Thuvander. The APT experiments were performed by Dr. Mattias Thuvander. Modelling work was performed by J. Moverare and the paper was written by me in cooperation with the co-authors.

Paper V: The work was planned by me. The experimental work was performed by me. The paper was written by me in cooperation with the co-authors.

Paper VI: The work was planned by me. The microscopy work was performed by Suhas Sreekanth. Mechanical testing was done by Prof. Christer Persson. The paper was written by me in cooperation with the co-authors.

Paper VII: The work was planned and the experiments were performed by me. Mechanical testing was done by Prof. Christer Persson. The paper was written by me in cooperation with the co-authors.

List of Acronyms and Abbreviations

AC- Air cooled/ing

APT- Atom probe tomography

DSC-Differential scanning calorimetry

EBSD- Electron back scattered diffraction

EDS-Energy Dispersive x-ray spectroscopy

El-Elongation

FC-Furnace cooled

LT-Longitudinal transversal

LSW-Lifschitz Slyozov Wagner

MA-Mill annealed

MA+A-Mill annealed +Aging

MA+LTA-Mill annealed + low temperature aging

PSD- Particle size distribution

S-Solutionising

SEM-Scanning electron Microscope

SHT- Standard Heat Treatment

ST-Short transversal

ST+A- Solution treated + Aging

TTH- Time Temperature Hardness

TTT-Time Temperature Transformation

UTS-Ultimate tensile strength

WQ-Water Quenched

YS-Yield strength

Table of Contents

Chapter 1

Introduction

Power generation and aerospace manufacturing industries are looking into new materials for critical applications in engines. Engines, which are the most complex element of an aircraft, houses several components and ultimately contribute to fuel efficiency. The concept of lean-burn engines has driven the demand for new high temperature materials that can sustain a higher temperature in comparison with Alloy 718, and should be castable and weldable as well.

Engine components were traditionally cast as single piece components, until recently where change in fabrication strategy has been made to meet the requirements for light weight and low cost technology. The new fabrication strategy opens up possibilities to adopt materials based on temperature needs but at the same time, challenges to tailor the heat treatment to suit the bi-metallic welds to be able to meet the desired property requirements still remain.

Heat treatments are generally done to alter the microstructure in a way as to achieve the desired mechanical properties. The microstructure-property relationship of a material is dependent on the processing history, as shown in the Figure 1. Alternative heat treatments (i.e.bi-metallic heat treatment) adopted to suit bi- metallic welds/structure are of interests to the industrial applications for understanding the microstructure-property relationship to suit such complex metallic structures.

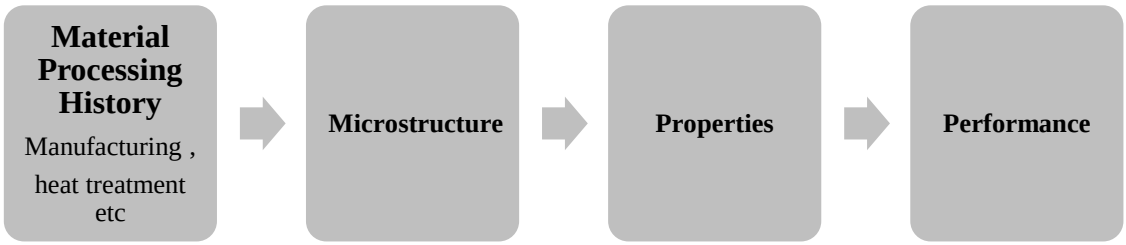

Figure 1 Structure-Property relationship in materials

One such material that can withstand hotter temperatures and be weldable and castable is a newly introduced nickel base superalloy Haynes 282 [1]. This alloy has recently gained huge interest in aerospace, gas and oil industries as one of the potential alloys for high temperature applications in gas turbine engines. Addition of new alloy to these applications, sets the need for systematic analyses on mechanical behavior, heat treatment and microstructural development when given the alternative heat treatment.

In the interest to explore high temperature fatigue life of Haynes 282 with alternative heat treatment, the project was initially aimed at studying the low cycle fatigue and thermomechanical fatigue behavior. However, in this process, it was found that Haynes 282 had lower yield strength and shorter fatigue life than expected at higher temperature. Characterization of the tested specimen showed differences in carbide morphology at the grain boundaries. As shown in Figure 2 (a) , alternative heat treatment showed presence of grain boundary carbides as films while the conventional heat treatment resulted in blocky (brick wall) structure.

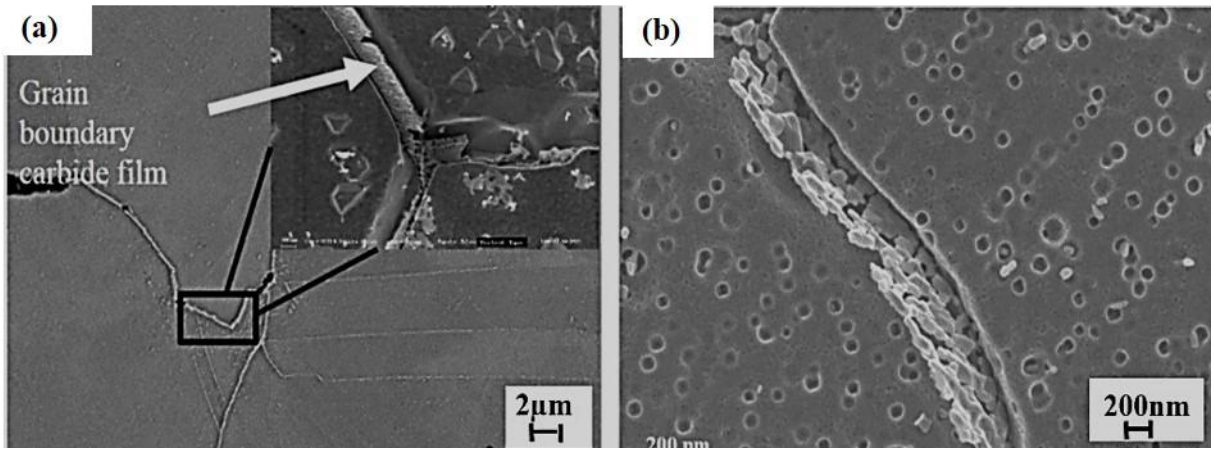

Figure 2 SEM images showing (a) Grain boundary carbides with film morphology, tested for fatigue at higher temperature (alternative heat treatment) (b) Grain boundary carbides with blocky morphology (conventional heat treatment)

Additionally, we see bimodal γ′ precipitates intragranularly, and γ′ precipitates and discrete carbides at the grain boundary. As shown in Figure 3 (a), alternative heat treatment shows presence of bimodal γ′ precipitates and γ′ at the grain boundaries. On the other hand, in the conventional heat treatment, as shown in Figure 3(b), we see uniform size of γ′ precipitates intragranularly and grain boundary with discrete carbides.

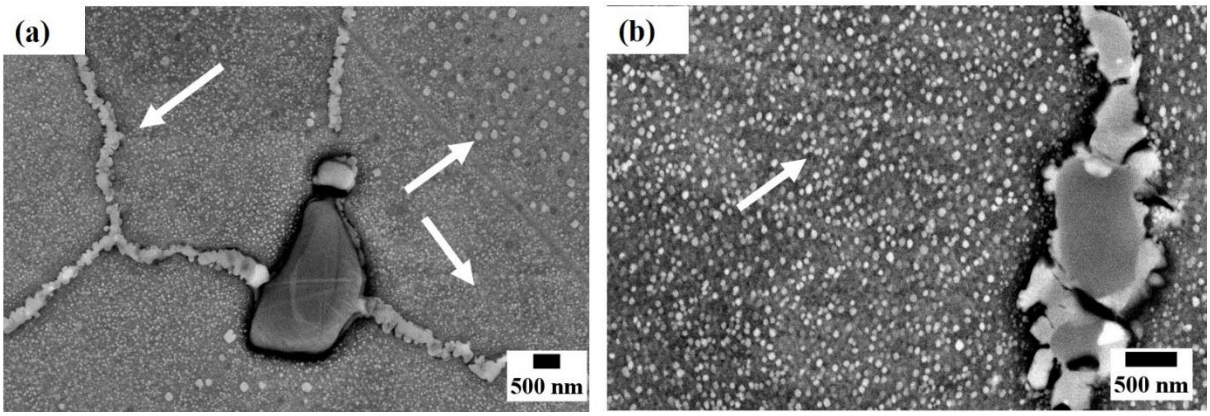

Figure 3 SEM image showing presence of (a) bimodal precipitation in alternative heat treatment (b) Spherical γ' prime precipitates.

Due to lack of enough literature on heat treatment and the indications that the material is sensitive to heat treatment parameters, the work within this project was focused on understanding the microstructural development of Haynes 282. The important aspect of this study was to correlate the microstructural changes evolved with different heat treatments to mechanical properties like tensile strength and ductility at room and high temperature.

1.2 Research Objective:

The main aim of this thesis is to investigate the sensitivity of Haynes 282 to heat treatment conditions that can affect the microstructure and mechanical properties both at room and high temperature. To achieve this, the objectives of the research work was

1. To understand the microstructural development in Haynes 282 and its sensitivity to temperature/time and cooling conditions.
2. To identify heat treatment parameter variation that can affect the microstructural features and the properties of this alloy both room and high temperature.
3. To identify the cause for variation in ductility of Haynes 282 forgings and sheets.

In order to answer these research questions, the organization of the work in this thesis is presented more in a logical approach, as shown in Figure 4, and not in the chronological order of the work performed.

Figure 4 Schematic illustration of the approach towards understanding microstructural development in Haynes 282with heat treatment

Chapter 2

Literature review

2.1 Introduction

After World War II, gas turbines became an important technology for their application in land-based power generation, the aircraft industry and other industrial processes [1, 2]. The materials formerly used in engine construction could not survive more than a few hundred hours at high temperatures. This created the need to develop new alloys to meet the demand for increased performance, reliability and emission in gas turbines.

Gas turbine engines deliver mechanical power using liquid fuel. In this process, these components are responsible for mixing the air and fuel, as well as creating combustion and producing high temperatures up to 1400 ˚C-1500 ˚C. This temperature window means that the materials and design for these components are very critical for such applications. Thus, such applications require the material to have excellent mechanical strength, resistance to thermal creep deformation and fatigue, good surface stability and resistance to corrosion and oxidation. This unusual class of material, known as superalloys, is attractive to scientists and researchers [2-4]. Figure 5 shows the temperature capability of superalloys since they were first introduced.

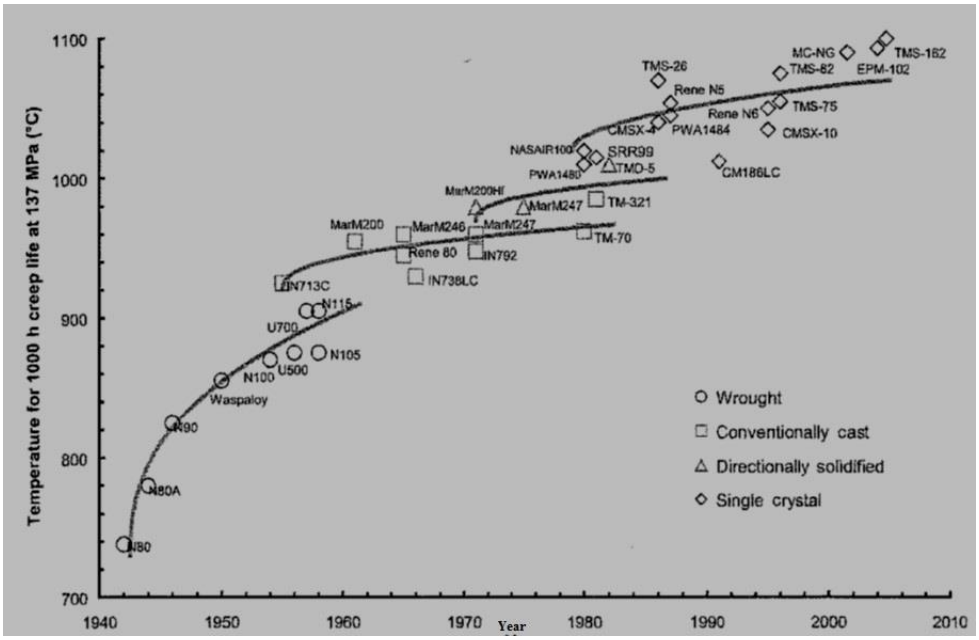

Figure 5 Temperature capability of superalloys since year of introduction [2]

Based on strengthening mechanism, superalloys are classified into three groups.

- Nickel-based (solid solution strengthening)
- Nickel-iron-based (precipitation strengthening)
- Cobalt-based (oxide dispersion strengthening)

Of the above, the nickel alloys find wide application in components used in aircraft engines, constituting over 50 % of their weight. The most common components are turbine blades, discs, seals, rings and casings of aero engines. The development of manufacturing processes produces alloys with uniform properties, fewer defects and less elemental segregation, thus making it possible to make significant improvements in mechanical properties [5]. Thus, the temperature capability of nickel alloys has now been improved considerably.

2.2 Nickel-based superalloys

Nickel-based superalloys are solution/precipitation strengthened alloys that contain many alloying elements. These are complex engineered materials because they involve precipitation of intermetallic phases, known as the gamma prime (γ') and gamma double prime (γ''), carbides such as MC (rich in Ti and Mo), $M_{23}C_6$ (rich in Cr) and other carbides such as M_6C (rich in Mo) and M_7C_3 [6-12]. The superior strength, high resistance to oxidation and corrosion, and creep properties of these alloys are essentially derived from the presence of these micro constituent phases [6]. The γ' phase is coherent with gamma matrix (γ) and is an important constituent that contributes to the strength, while the carbides are incoherent to the matrix and are present at grain boundaries and intragranularly in the nickel alloys [2]. The alloying elements determine the composition of the superalloy while the heat treatment is important for optimising the properties. Each of them is discussed later in this section.

2.3 Role of alloying elements

The matrix consists principally of Ni, Co, Cr and refractory metals such as Mo; the relative amounts of all of these are determined by other elements such as Al, Ti, C and B which react to form precipitating phases. Alloying elements and their importance in nickel-based superalloys has been reported widely in literature and is summarised in Table 1. Some of the critical elements such as Al and Ti are important for fabricability [13]. Lower levels of Mo (1 or 2 %) are deleterious as they can affect the creep strength of the material, while a minimum of 15%-20 % of Cr is desirable for hot corrosion properties [7].

Table 1 Role of alloying elements in nickel alloys

Element	Amount found in Ni-based/Fe-Ni-based alloys (wt%)	Effect
Cr	5-25	Oxidation and hot corrosion resistance; carbides; solution hardening
Mo-W	0-12	Carbides; solution hardening
Al-Ti	0-6	Precipitation hardening; carbides
C	0.02-0.10	Forms carbides
Co	0-20	Affects amount of precipitate, raises γ′ solvus
Ni	Rest	Stabilises austenite; forms hardening precipitates
Ta	0-12	Carbides; solution hardening; oxidation resistance
Nb	0-4	Carbides; solution hardening; precipitation hardening

2.4 Heat treatment of Ni-based superalloys

Microstructure is fundamental to attaining the required properties in superalloys [14]. The relationship between microstructure and resulting mechanical properties is widely studied in both wrought and cast superalloys [15-29]. To derive its high temperature strength, and properties during in-service conditions, it is essential to control the microstructure through the use of precipitated phases [15].

Ni-based superalloys are normally supplied in solution-treated condition because they have an optimum combination of properties for room temperature fabrication and elevated temperature service. However, by heat treatment it is possible to achieve

- Precipitation hardening
- Desired precipitation of carbide
- Optimum grain size through grain growth (in wrought and cast alloys), and through recrystallisation and grain growth along with mechanical deformation (forging)

Figure 2 shows a schematic diagram for heat treatment in superalloys in general.

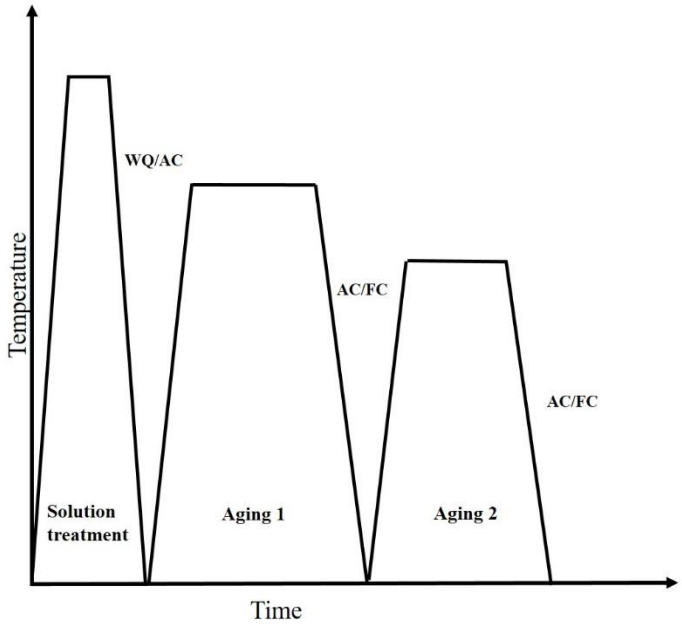

Figure 6 Schematic sketch of heat treatment steps in superalloys

In case of wrought Ni-based superalloys, the solution is treated to dissolve nearly all γ′ and carbides other than the stable MC carbides. Typical solution treatments are in the range of 1050 ˚C to 1200 ˚C followed by either air-cooling or water quenching. On quenching a supersaturated solid solution is formed. The following two-step ageing process is carried out to precipitate γ′; the first step often being carbide stabilisation while the second step completes the precipitation of γ′.

In order to achieve desired properties, the heat treatment process must be optimised. Factors such as cooling rate [16], ageing temperatures and time [19], and solutionising temperatures [26] are some of the heat treatment parameters that can alter the morphology of precipitated phases and thereby affect the properties of these alloys.

2.4.1 Carbide precipitation

One of the basic mechanisms for strengthening wrought Ni-based alloys is carbide precipitation. The type of carbides formed depends on the alloying elements, while its morphology and distribution are affected by heat treatment. The temperatures and time for carbide precipitation are often carefully considered because these carbides undergo complex reactions, which can generate detrimental and beneficial effects by either changing to different forms of carbides or by changing their morphology. Carbides present at the grain boundaries in a desired morphology exhibit good creep strength and ductility, by inhibiting grain boundary sliding [6, 30].

Since carbide precipitation and distribution is very important in Ni-based alloys, the influence of carbide morphologies, type and distribution to high temperature properties have been studied and reported in literature [29-50]. The three main forms of carbide reported in literature for Ni-based alloys are MC, $M_{23}C_6$ and M_6C (where M stands for metallic element). Table 2 shows the different morphologies of carbides formed in Ni-based alloys.

Table 2 Morphology of different carbides in Ni-based alloys

Carbides	Morphology
MC (Ti and Mo-rich)	Blocky, discrete, script
M_6C(Mo-rich)	Discrete, acicular, platelets
$M_{23}C_6$(Cr-rich)	Film, blocky, cellular, zipper

MC carbides are formed at higher temperatures during melting. They are generally insoluble carbides which precipitate with irregular shapes and are believed not to influence the properties unless they are segregated [39, 49]. On thermal exposure, the carbides can undergo decomposition to form different stabilised states.

$$MC + \gamma \rightarrow M_6C + \gamma'$$

$$MC + \gamma \rightarrow M_{23}C_6 + \gamma'$$

M_6C carbides are formed in the intermediate temperature range and enhance the property of the material only if present in the desired discrete morphology. They are generally preferred to $M_{23}C_6$ carbides, because of their stability at higher temperatures. [38]

$M_{23}C_6$ usually precipitates at the grain boundaries in chromium-rich alloys as irregular and discontinuous particles at temperatures between 760 ˚C-980 ˚C. Continuous films of carbides can affect ductility and stress ruptures of the material are avoided in this form [21, 32].

2.4.2 Gamma prime precipitation

Gamma prime precipitate is the principal strengthening phase in Ni-based alloys. The γ′ precipitation is generally formed during cooling from the first ageing step or during the second ageing step [30]. Temperature, time and cooling rates in heat treatment can affect the γ′ precipitation [51-54]. The morphology, distribution and volume fraction of γ′ play a very important role, not only for strength but also for determining fabricability [6, 13]. They are seen as cuboidal and spherical morphologies in different Ni-based alloys. The principal alloying elements that form these precipitates are Al and Ti. The γ′ strengthened alloys have increased need for easy fabricability so that they can be easily welded and formed into various shapes. Hence, their addition is carefully balanced in order to achieve better fabricability and optimum hardening [30].

2.4.3 Isothermal transformation in superalloys

Structures developed in nickel-based superalloys as a result of heat treatment are metastable, as they change with time upon exposure to elevated temperatures. [11] Hence, isothermal transformation diagrams are considered as roadmaps to work out the presence of different phases under a given/time temperature conditions [55]. Isothermal transformations for different nickel alloys [56-62] presented in literature are used for understanding phase stability in these alloys. Local inhomogeneity, thermo-chemical processing and stress can either alter the volume fraction and size distribution on nitrides, carbides and carbonitrides or shift the transformation forward [55]. Furthermore, chemical composition can shift the transformation curves to shorter times in solute-rich areas, generating non-uniform phase precipitation. Although isothermal transformation behaviour, is very specific in terms of reported chemical composition, size and processing and is different from the precipitation response encountered during the multistep heat treatment, it still serves as a good tool for material engineers.

Chapter 3

Haynes 282–A new fabricable superalloy

3.1 Introduction to Haynes 282

Haynes 282 is a corrosion-resistant and high creep-strength Ni-based superalloy, which was developed by Haynes International in 2005 with the aim of making a weldable Ni-based superalloy to replace Waspaloy for use in making different components for the aeroengine industry. Hitherto, Waspaloy has been considered as a good Ni-based superalloy in the intermediate temperature range for aero-engine applications but it is difficult to use it for making flat products and, in particular, it is not weldable. [1]. Hence, Haynes 282, a new wrought γ′ strengthened alloy, has been attracting interest for various applications due to a combination of properties like creep strength, thermal stability and fabricability [1, 13, 63-65]. The chemical composition of this alloy is as shown in Table 3.

Table 3 Chemical Composition (wt %) of Haynes 282 alloy

Ni	Cr	Co	Mo	Ti	Al	Fe	Mn	Si	C	B
Bal	19.44	10.22	9.42	2.15	1.44	0.92	0.06	0.07	0.067	0.004

The conventional heat treatment of this alloy is 1010 °C/2h/air-cooled (AC) and 788 °C/8h/AC. As shown in Figure 3, the conventionally heat-treated alloy has spherical ′γ precipitates and discrete carbide morphology at the grain boundaries.

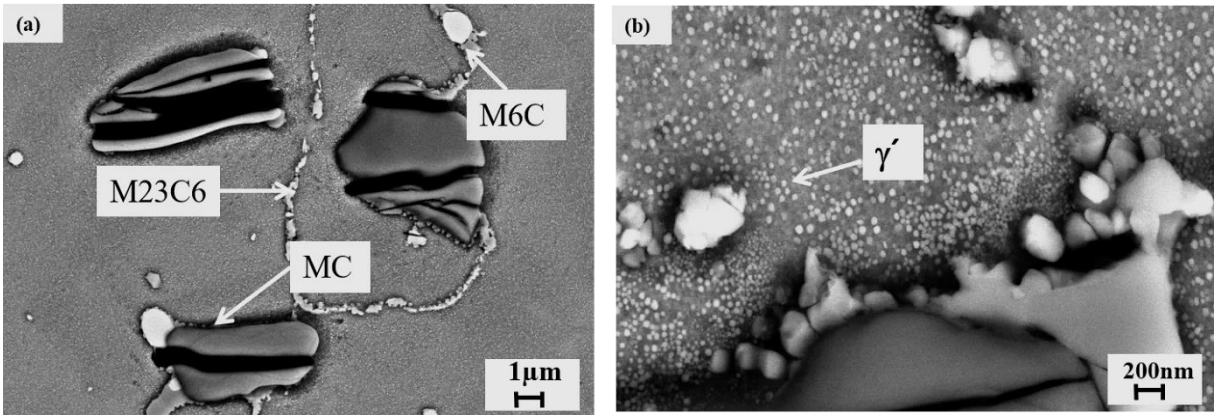

Figure 7 Scanning electron microscope (SEM) images of conventional heat-treated Haynes 282 alloy showing (a) carbides (b) γ'

In literature [1], Haynes 282 has been presented as having improved formability under solution-treated conditions compared with other γ′ containing alloys such as Waspalloy and R-41. More recently, most contributions in the literature on Haynes 282 have focused on castability and microstructure evolution [66-70], weldability and microstructure [71-79], creep [80-82] and low cycle fatigue [83-84] under conventionally heat-treated conditions because these behaviours are crucial for aerospace applications. Furthermore, the oxidation and corrosion behaviour [88] and sensitivity to hydrogen embrittlement [89] of Haynes 282 have been also studied and the alloy has been found to show resistance to such aggressive environments.

Jablonski et al. evaluated the effect of high Al and Ti in Haynes 282 with fixed gamma prime content [90] on its creep and tensile properties. The authors reported that the alloy is insensitive to changes in the content of these elements within the alloy specification. K. Barat et al., studied the microstructure and its evolution during different thermal and thermo-mechanical treatments in forgings [86] and reported the presence of M_3B_2 boride and carbides such as $M_{23}C_6$ and M_6C and the absence of TCP phases such as Mu and sigma. On the other hand, in a study on microstructural evolution in fusion welds, the authors reported the presence of continuous films of grain boundary precipitates of $M_{23}C_6$ and μ, on long-term exposure (to what? What kind of exposure?). [82] In a recent study, isothermal precipitation kinetics in Haynes 282 has been investigated by using small-angle X-ray scattering (SAXS) and wide-angle X-ray scattering (WAXS), and it has been found that the peak hardness of gamma prime in the material is strongly dependent on the ageing temperature [91].

Y. Yang et al. reported the presence of gamma prime in a star morphology under air-cooled conditions and its sensitivity to variations in heat treatment conditions, which significantly affect microstructural development and potentially the properties of the material [70]. Most contributions in existing literature are centred on the standard two-step heat treatment. Therefore, we were interested in exploring alternative heat treatment conditions. There was a need to understand the potential microstructural and property change that can occur on alternative heat treatment conditions suitable to bimetallic welds. Knowledge of heat treatment conditions is important in order to tailor the properties and performance of the alloy so as to be able to adopt materials based on temperature requirements and still be able to meet the desired property requirements. Current work on microstructural evolution and mechanical properties is therefore focused on bridging this knowledge gap and to gain understanding about the sensitivity of Haynes 282 to heat treatment conditions.

3.2 Forms of Haynes 282

During this work, there was the chance to see microstructures of Haynes 282 forgings, bars and sheets. As shown in Figure 8a, the forgings showed the presence of banded structures with bimodal distribution of grain size and carbide stringers. In the case of the bars, uniform grain

size distribution with uniformly distributed carbides was seen (Figure 8b) while, as shown in Figure 8c, the sheet material showed the presence of carbide stringers in the rolling direction with uniform grain size distribution.

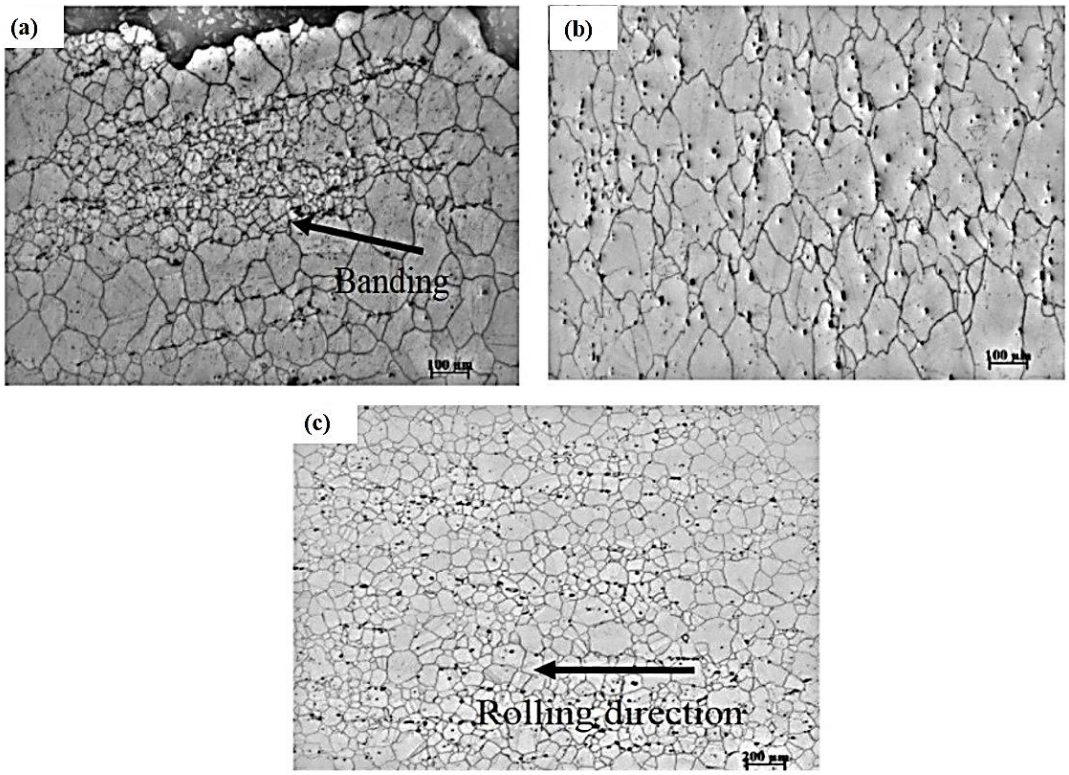

Figure 8 Optical microstructure of Haynes 282(a) forgings (b) bars (c) sheets

The mechanical test results on sheets and bars showed differences in ductility with the heat treatment adopted here. Hence, the work on microstructural evolution and mechanical properties is focused on sheet material of 3mm thickness.

3.3 Heat treatment of Haynes 282

3.3.1 Standard heat treatment

The typical solution-annealing temperature for Haynes 282 sheet is from 1120 ˚C to 1149 ºC.

After component fabrication, two-step age-hardening treatment is performed at 1010 ºC/ 2h /AC + 788 ºC/ 8h / AC to attain the high strength condition.

3.3.2 Alternative heat treatment

In the current work, an alternative heat treatment was performed in order to understand material behaviour and strength capabilities when it is in use with complex structures involving different materials. In the alternative heat treatment, the initial two steps were omitted and only the last step of the heat treatment was performed on the solution-annealed material, which resulted in

poor properties. The alternative heat treatment is subject to a non-disclosure agreement and hence not mentioned anywhere in this report.

3.4 Sensitivity to Temperature/Time and cooling conditions

In nickel alloys, a good combination of properties is achieved due to precipitation of gamma prime (γ′) and grain boundary carbides (mainly $M_{23}C_6$ and M_6C) formed during heat treatment [2-4]. To adequately understand the influence of microstructure on high temperature performance, it is critical to understand the nature of precipitation during and after heat treatment.

3.4.1 Gamma prime on cooling

Gamma prime (γ′) solvus in Haynes 282 is reported to be approx. 997 ºC [1] while that seen from JmatPro simulations is approx. 1003 ºC. As is evident from the SEM micrographs shown in Figure 9, no γ′ precipitates were seen in a mill-annealed state in Haynes 282 sheet material.

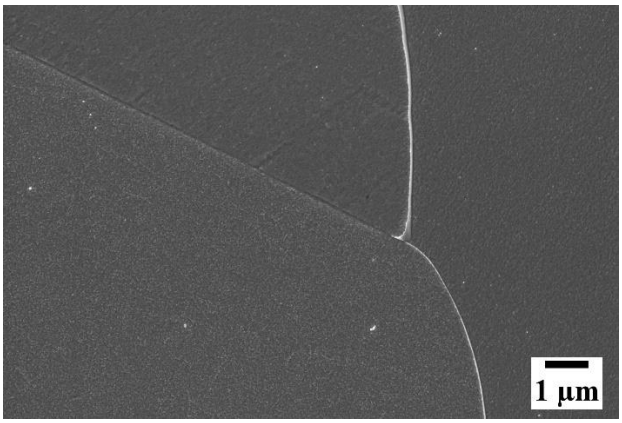

Figure 9 SEM image of mill-annealed specimen showing no presence of γ′

Furthermore, in earlier studies, bimodal precipitation of γ′ (cf. Figure 3), and a change in γ′ morphology were observed on additional solution-heat treatment at 1120 ºC for 2 h [92]. This indicates that it is important to understand the gamma prime (γ̀) precipitation during different heat treatments with varying cooling rates and initial starting conditions i.e. mill- annealed state. The aim of this study is therefore to systematically understand the γ′ precipitation on cooling from different heat treatment temperatures and in the mill-annealed condition.

3.4.2 Isothermal transformations

The morphology, size and distribution of the precipitated phases such as the γ′ and grain boundary carbides are a function of heat treatment parameters like the temperature-time and cooling rate conditions. As seen in Figure 2, the grain boundary carbides appear in two different morphologies. A small drop from 1010 ºC to 996 ºC showed a change in morphology and distribution of precipitated γ′ phase and in grain boundary carbides [92]. This led to the study on phase stability of precipitated phases such as γ′ and grain boundary carbides in Haynes 282 under different isothermal temperature/time conditions.

3.5 Sensitivity to heat treatment

As stated in section 1.1, Haynes 282 showed sensitivity to heat treatment parameters, resulting in different morphologies of carbides at the grain boundaries and bimodal precipitation of γ′ precipitates (cf. Figure 3). It was therefore important in this study to correlate the microstructural changes to mechanical properties such as strength and ductility at different heat treatment temperatures.

3.5.1 Variation in heat treatment parameters

As an initial step, a preliminary study on the standard two-step ageing was conducted, in order to determine how different aspects of the heat treatment influences the morphology of microstructural features and its subsequent impact on room temperature properties of strength and ductility in Haynes 282. Based on the results from the preliminary study, three parameters; initial state of the material, solutionising parameters and carbide stabilisation parameters were seen to affect the room temperature properties by changing both carbide morphologies and γ′ precipitation. To develop a better understanding of the microstructural development, each of these identified parameters were systematically studied in this work.

3.5.1.1 Variation in solution treatment parameters

In the earlier work, solution treatment at high temperature for two hours was seen to affect the ductility of the material. It introduced grain growth and changed the morphology of grain boundary carbides and γ′ during subsequent ageing. In order to understand its influence on microstructure, a systematic microstructural investigation was performed after each heat treatment step. A set of heat treatments with a combination of these parameters were also tested to study the influence of solution treatment parameters on mechanical properties.

3.5.1.2 Variation in carbide stabilisation parameters

The carbide stabilisation step is the first step of the ageing treatment and aims primarily to precipitate the grain boundary carbides. This is followed by the second ageing step at 788 ºC for eight hours, where the γ′ precipitation occurs. To understand the influence of these variations on microstructure, a systematic microstructural investigation was performed after each heat treatment step. Additionally, mechanical testing was carried out on a set of heat treatments with a combination of these parameters to study the influence of carbide stabilisation parameter variations on tensile properties at room temperature and at 730 ˚C.

3.6 Anisotropic ductility

Haynes 282 forgings showed variations in room temperature ductility. The mechanical test results on forging showed ductility variations from 12 % to 24 % in the short transversal direction while it remained unaffected in the longitudinal direction. Hence, this part of the concluding work focuses on understanding the ductility variations in Haynes 282 forgings after heat treatment.

Chapter 4

Experimental Details and Analytical Techniques

4.1 Material

As discussed in Chapter 3, Haynes 282 sheet material of 3mm thickness has been used in this study. The heat treatments were performed on mill-annealed sheet with a grain size of ASTM 3.5. In the course of the anisotropic study, we also had the chance to check on other forms of Haynes 282 such as forgings and bars. The typical composition of Haynes 282 is as shown in Table 2 in Chapter 3.

4.2 Heat treatment

The Haynes 282 sheet, as received, was heat-treated in air in a chamber furnace. The sheet was cut into small pieces by water jet cutting and was subjected to heat treatment schedules, as mentioned below.

4.2.1 Gamma prime on cooling

To understand the precipitation of γ′ on cooling, three different starting conditions were investigated: the mill-annealed state and two states receiving solution treatment at 1120 °C for 30 min followed by air-cooling and water quenching respectively

4.2.2 Isothermal transformation

In the isothermal transformation study, 10×10×3 mm^3 samples were cut from the sheets directly and heat-treated in air using a box furnace in a temperature range of between 650 °C and 1120 ºC. In a temperature range of between 650 °C and 980 °C, heat treatments were performed for periods ranging from 2 min to 98 h whereas at higher temperatures (between 1000°C and 1120 °C), times from 2 min to 2 h were used.

4.2.3 Sensitivity to heat treatment

In the initial heat treatment study, the temperatures were varied around the standard heat treatment conditions, as described in Table 4.

Table 4 Heat treatment schedule

Referred as	**Solution treatment**	**Ageing step 1**	**Ageing step 2**
Solution treatment + ageing (ST+A)	1120 ºC / 2h (WQ*)	1010 ºC / 2h (FC**)	788 ºC / 8h (FC)
Mill- annealed + ageing (MA+A)	-	1010 ºC / 2h (FC)	788 ºC / 8h (FC)
Mill- annealed + low temperature ageing (MA+LTA)	-	996 ºC / 2h (FC)	788 ºC / 8h (FC)

*WQ- water-quenched ** FC – furnace-cooled

4.2.3.1 Variation in solution treatment parameters

In this part of the study, the solution treatment (first step shown in Figure 10) parameters were varied according to Table 5, and this was followed by the standard two-step ageing.

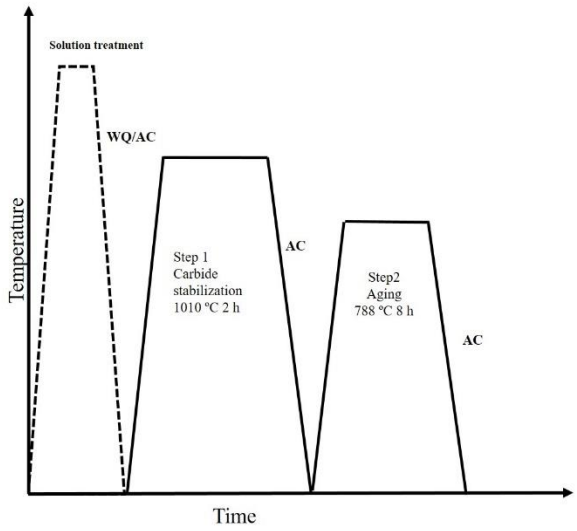

Figure 10 Schematic diagram of heat treatment where solution heat treatment is varied

Table 5 Heat treatment variables for microstructural study with varying solution treatment parameters

Solution treatment Parameters	
Temperature	1080 ˚C, 1100 ˚C, 1120 ˚C
Time	15 min, 30 min, 60 min
Cooling rate	Air-cooling (AC), Water-quenching (WQ)

Standard heat treatment (SHT) *1010 ˚C/2 h/AC+ 788 ˚C/8 h/AC*

Further, a set of heat treatments with a combination of these parameters was tested for mechanical testing to study the influence of solution treatment parameters on tensile properties. Table 6 below shows the heat treatment matrix for mechanical testing at room temperature and at 730 ˚C.

Table 6 Heat treatment for mechanical testing

Heat treatment	Solution treatment parameters
S1	1120 ˚C -120 min WQ +SHT
S2	1120 ˚C -30 min WQ + SHT
S3	1120 ˚C -30 min AC + SHT
S4	1100 ˚C -30 min WQ + SHT
S5	1100 ˚C -60 min WQ + SHT
S6	No solution treatment + SHT

*SHT: 1010 ˚C -2 h AC+788 ˚C-8 hAC

4.2.3.2 Variation in carbide stabilisation parameters

The carbide stabilisation step is the first step of the ageing treatment (Figure 11), which aims primarily to precipitate the grain boundary carbides. This is followed by the second ageing step at 788 ºC for 8 h.

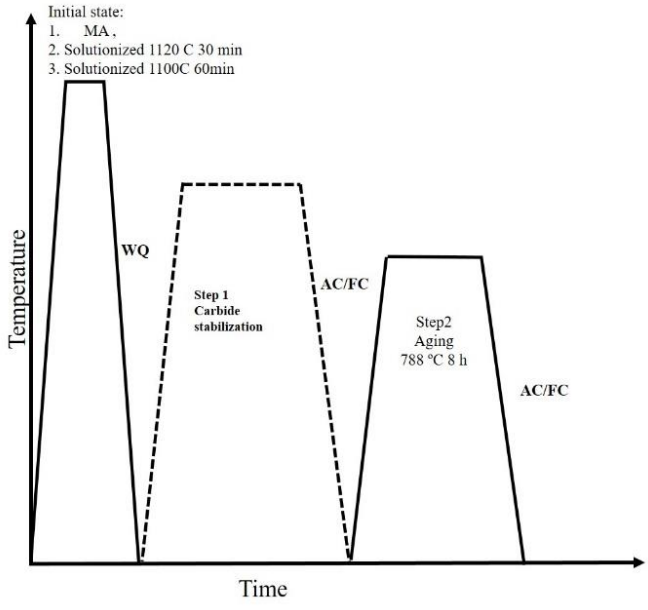

Figure 11 Schematic diagram of heat treatment where carbide stabilisation heat treatment is varied

Direct ageing (without carbide stabilisation step), as shown in Figure 12, was also performed. In order to understand the influence of carbide stabilisation parameters, an initial microstructural study was carried out by varying the heat treatment parameters on three different initial states of the material (Table 7).

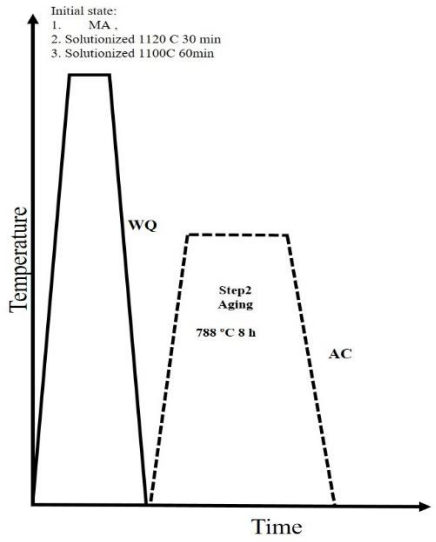

Figure 12 Schematic diagram of heat treatment showing direct ageing without the carbide stabilisation step

Table 7 Heat treatment variables for microstructural study with varying carbide stabilisation parameters

Initial states	**Carbide stabilisation Parameters**		**Standard Ageing (A)**
MA / 1120 ˚C-30 min WQ/ 1100 ˚C-60 min WQ	Temperature	1024 ˚C, 1010 ˚C, 996 ˚C	788 ˚C/8 h/AC
	Time	30 min, 60 min, 480 min	
	Cooling rate	Air-cooling (AC) / Furnace cooling (FC)	
Direct Ageing			
MA/1120 ˚C-30 min WQ/ 1100 ˚C-60 min WQ			788 ˚C/8 h/AC

*Direct Ageing is considered as final ageing without carbide stabilisation step. * MA: Mill-annealed *Standard heat treatment (SHT) *1010 ˚C/2 h/AC+ 788 ˚C/8 h/AC*

Further, a set of heat treatments with a combination of these parameters was tested to study the influence of the carbide stabilisation treatment parameters on mechanical properties (tensile properties). Table 8 shows the heat treatment matrix for mechanical testing at room temperature and 730 ˚C.

Table 8 Heat treatment parameters for mechanical testing

Heat treatment	**Solutionising parameters (S)**	**Carbide stabilisation parameters + Ageing(A)**
S+1010 ˚C 1h AC+A	1100 ˚C-60 min WQ	1010 ˚C -1h AC+A
S+996 ˚C 1h AC+A	1100 ˚C -60 min WQ	996 ˚C -1h AC+A
S+1010 ˚C 1h FC+A	1100 ˚C -60 min WQ	1010 ˚C -1h FC+A(FC)
S+996 ˚C 1h FC+A	1100 ˚C -60 min WQ	996 ˚C -1h FC+A(FC)
S+A	1100 ˚C -60 min WQ	A
MA+A	– –	A

*S: 1100 ˚C-60 min WQ A: 788 ˚C-8 h AC *MA: Mill-annealed

4.2.4. Anisotropic ductility

In the anisotropy ductility study on forged specimens, heat treatment was performed according to AMS 5951.

4.3 Test Methods

4.3.1 Mechanical Testing

Tensile specimens were cut by water jet cutting and these were tested at room temperature in an MTS servo hydraulic machine in accordance with ASTM standard E8 [93] and at high temperature in accordance with ASTM E21 [94].

Forgings: The tensile testing was performed by GKN aerospace in accordance with ASTM standard E8

4.3.2 Hardness

Hardness measurements were performed to determine the ageing of the material. The Vickers macrohardness test was performed using a 10kg load in accordance with ASTM standard E92 [95], and an average of five indentations were reportedly produced.

4.3.3 Microscopy

A Leitz DMRX light optical microscope equipped with Axio-vision software was used to study the microstructure on polished and etched samples. An SEM LEO 1550 was also used for fractographic analysis and to observe the γ′ precipitates and carbide morphology under different heat-treated conditions.

4.3.4 Atom Probe Tomography

Atom probe tomography (APT) is the material analysis technique offering extensive capabilities for both 3D imaging and chemical composition measurements at the atomic scale with a resolution limit of around 0.1 nm-0.3 nm in depth and 0.3 nm-0.5 nm laterally. In this study, needle- shaped APT samples were prepared from the blanks by electropolishing using standard solutions and conditions for nickel alloys and the material was characterised using the atom probe instrument LEAP 3000X HR, from Imago Scientific Instruments.

4.3.5 Differential Scanning calorimetry

Differential scanning calorimetry (DSC) was performed using the Netzsch STA 449 F1 Jupiter ® analyser. Discs of 4.5 mm diameter and 1 mm thickness, with a mass of approximately 100 mg-200 mg, were prepared and the measurements were taken for the selected heat rate (10 ºC/min) over the temperature range RT-1200 C and gas flow rate (50 ml/min argon). The solvus temperatures were evaluated using Netzsch Proteus software.

4.4 JmatPro Simulations

JmatPro calculation software version 9.0 of the Ni- database was used for the simulation of the thermodynamic phases formed, and the phase transformation for γ′and carbides in Haynes 282.

Chapter 5

Results and Discussion

5.1 Mill-annealed condition

Initial characterisation of the mill-annealed state of the material, used in the major part of this work, is described in this section. The composition is as given in Table 9. As seen in the optical micrograph in Figure 13a, the grain size was around ~100 µm with MC carbides present along the rolling direction both inter and intragranularly

Table 9 Chemical composition of Haynes 282 sheet material

Ni	Cr	Co	Mo	Ti	Al	Fe	C	B	P	S	Si
Bal	19.52	10.11	8.67	2.24	1.48	1.0	0.053	0.005	0.002	0.002	0.05

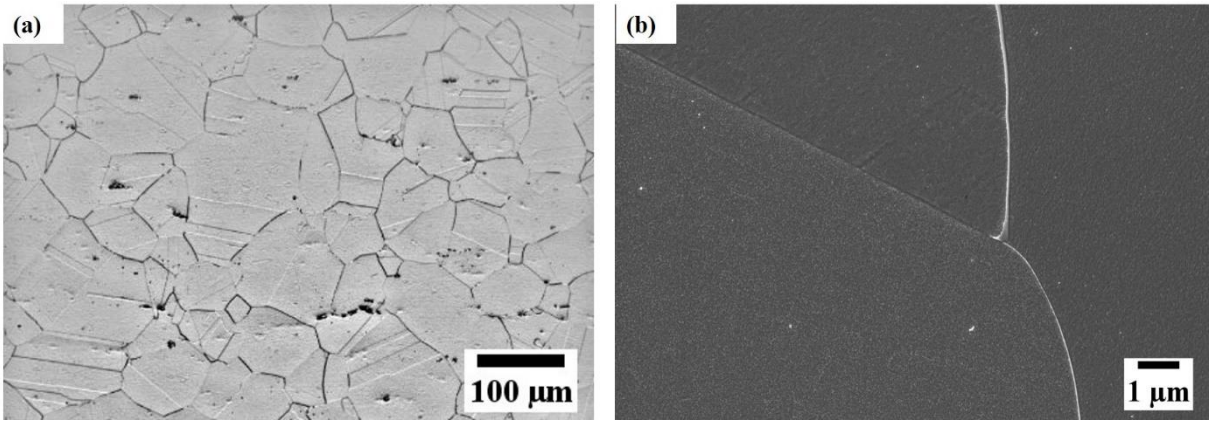

Figure 13 (a) As-received optical microstructure of Haynes 282 sheet; grain structure and presence of inter and intragranular MC carbides (b) SEM shows no traces of γ´ in the grains and grain boundary free from carbides.

SEM image in Figure 13b shows the occasional presence of secondary carbides at grain boundaries and the hardness was measured at approx. 209 HV. The mechanical test at different temperatures was performed and the properties are summarised in Table 10. The tensile strength shows strong dependence on temperature. It can be seen that the yield strength falls at 650 ºC and then starts to increase at 730 ºC. The ultimate tensile strength shows a decrease with temperature. The elongation is 65 % at 650 ºC, which subsequently decreases at 730 ºC.

Table 10 Mechanical properties of as-received state at different temperatures

MA	YS	UTS	%El
RT*	372	834	64
650	302	658	65
730	428	608	28

- *Data from supplier

The fracture surface of these tested specimens is as shown in Figure 14. The fractography structure observed shows evidence of void coalescence and ductile fracture at all temperatures, however the size of the dimples seems to vary in all three tested conditions. The maximum ductility observed at 650 ºC can be attributed to the fine dimples present on the fracture surface, while the dimples at 730 ºC were larger in size, which is evidence of microvoid nucleation and growth during plastic deformation.

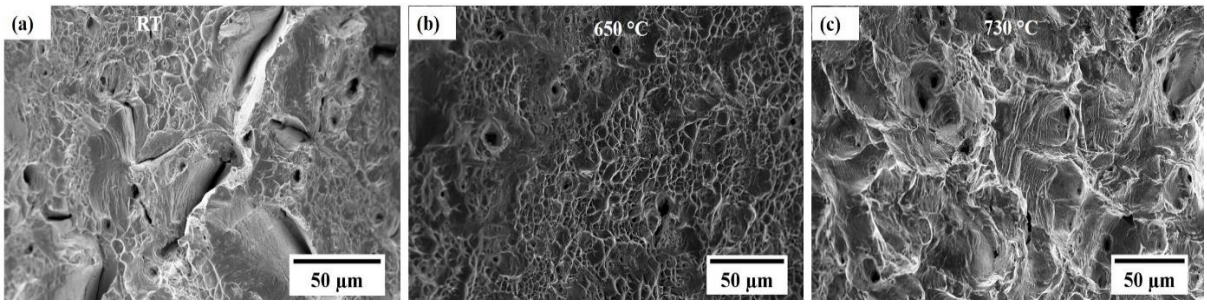

Figure 14 Fractographs of tensile specimen tested at different temperatures (a) RT (b) 650 ºC and (c) 730 ºC

5.2 JmatPro simulations

JmatPro software version 9.0 using nickel database was used for the thermodynamic simulations and the phase transformations in Haynes 282. Figure 15 shows the thermodynamic equilibrium calculations in Haynes 282. As seen in Figure 15, the precipitation of the grain boundary carbides $M_{23}C_6$ is and M_6C are approx. 860 ºC and 1180 ºC respectively. Furthermore, the γ´ precipitates are just above 1000 ºC.

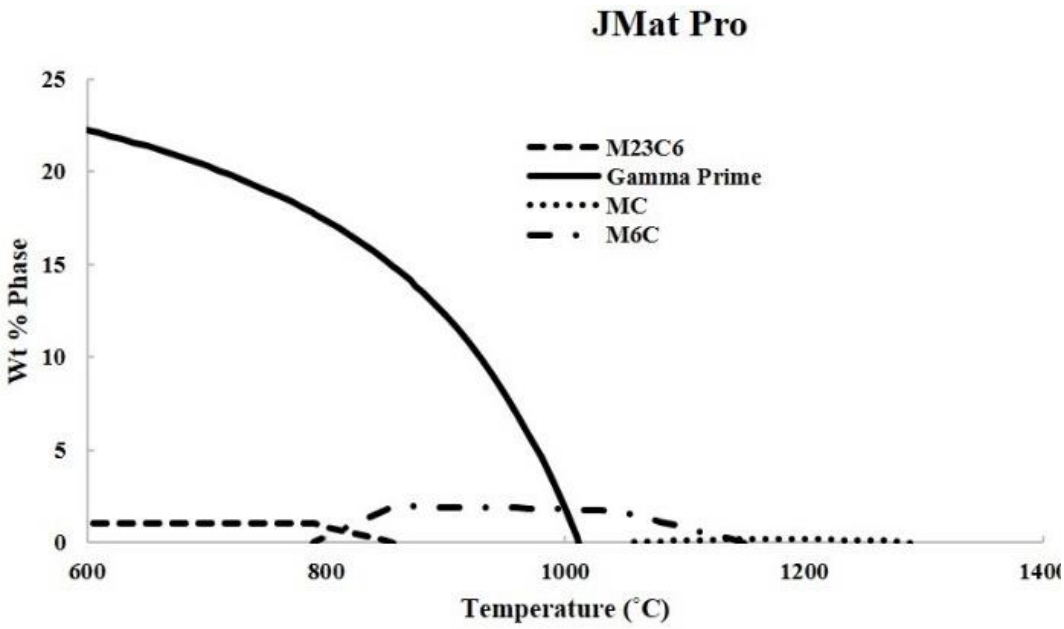

Figure 15 Calculated phase fractions Vs temperature diagram for Haynes 282

Figure 16 shows the phase transformation in Haynes 282. As seen in Figure 16, the formation temperature of phases such as $M_{23}C_6$, M_6C and γ′ is not the same as seen in the thermodynamic calculations in Figure 15, for 0.1 % transformation. The γ′ solvus was found to be 1003 ºC, while that reported in literature is 997 ºC [1]. The nose of the transformation curves shows that the γ′ formation time is shorter while for carbides the formation time is approx. 2 min.

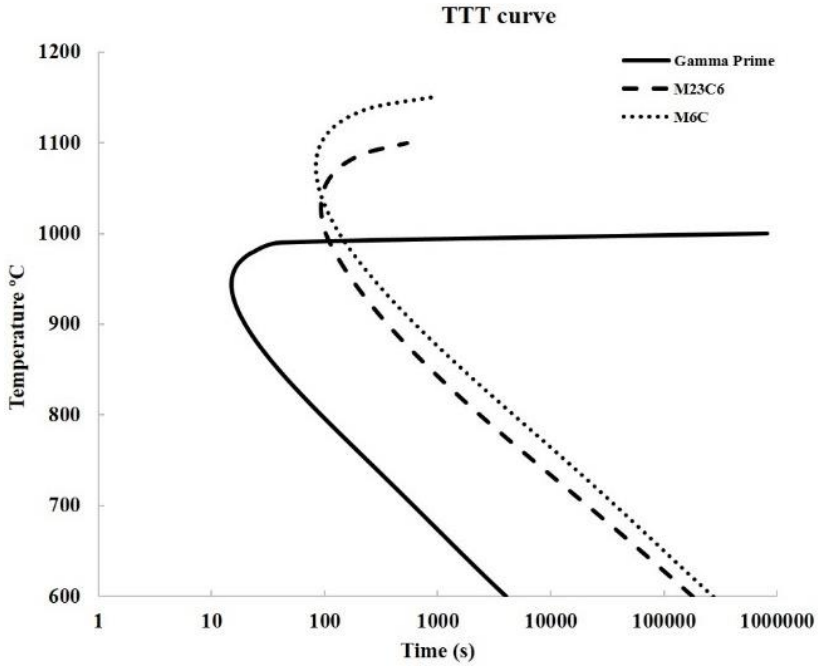

Figure 16 Predicted phase transformation in Haynes 282 using JMatPro

5.3 Sensitivity to Temperature/Time and cooling conditions

5.3.1 Gamma prime on cooling

In order to understand the nature of γ′ precipitation during and after heat treatment, three different initial states of the material, i.e. mill-annealed condition, solution-treated, and solution-treated as well as the carbide stabilised state were subjected to cooling at different rates. Figure 17 shows the heat treatment chart for these conditions. Each of these states were investigated for γ′ precipitation by systematic analysis through SEM, hardness and atom probe tomography (APT).

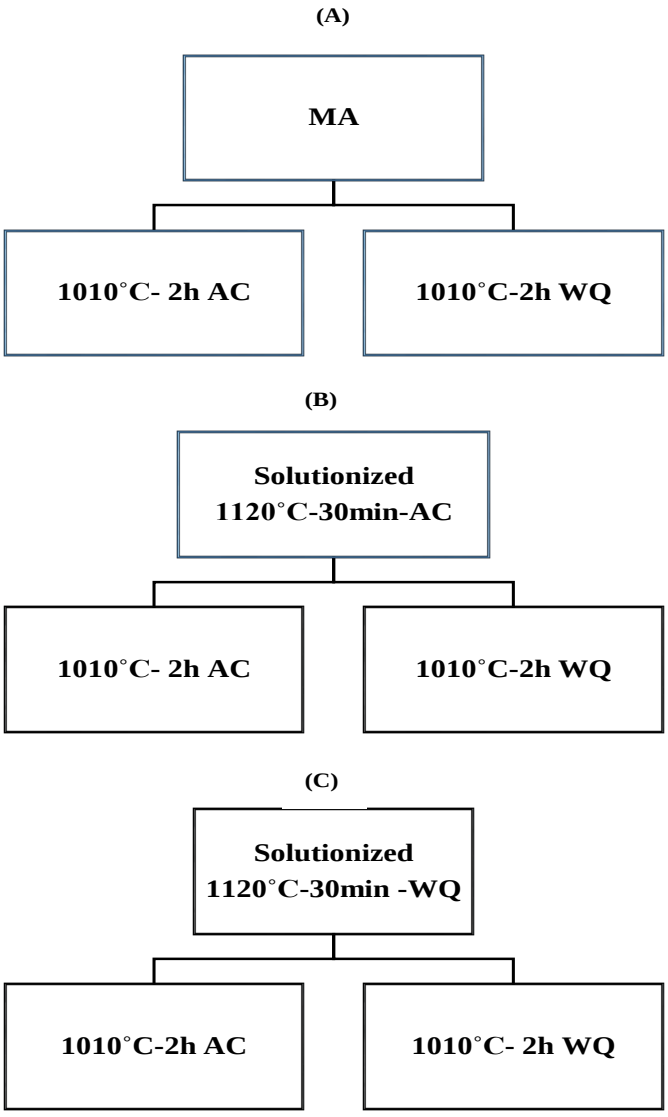

Figure 17 Heat treatment chart (A) Mill-annealed (B) Solutionised and air-cooled (C) Solutionised and water-quenched. Each of the conditions were subsequently aged, with different cooling rates from the ageing temperature. (AC: Air-cooled WQ: Water-quenched MA: Mill-annealed).

Figure 18 shows the SEM images of grain boundary carbides and the absence of γ′ precipitates with different heat treatment conditions as seen in Figure 17. The results from this investigation shows small amount of grain boundary carbides in the mill-annealed state, which are removed during solution treatment. The carbide stabilisation treatment does indeed produce a distribution of discrete carbide particles at the grain boundaries, while no γ′ precipitation is seen in the grain boundaries, and in none of these cases intra-granular γ′ was observed.

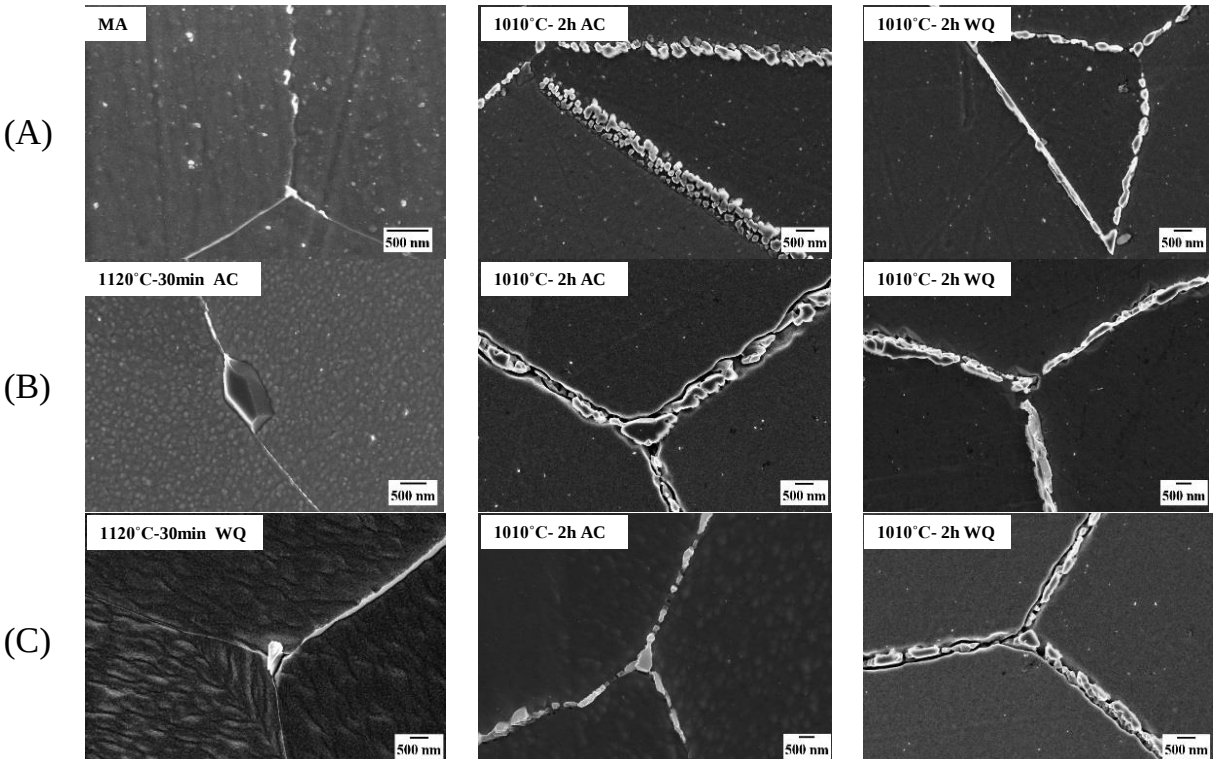

Figure 19 SEM images showing the presence of grain boundary carbides and the absence of γ′ precipitates with different heat treatment conditions (A) Mill-Annealed (B) Solutionised and air-cooled (C) Solutionised and water-quenched

The hardness of these heat-treated specimens is as seen in Figure 19, shows a decreased hardness from the mill-annealed state after solution treatment and water quenching. However, an increase in hardness is observed after air-cooling from the solution treatment temperature. As no grain growth occurred during the solution treatment, this suggests that dissolution of cooling-induced precipitates in the mill-annealed state is responsible for the decrease in hardness, and that the precipitation process is fast enough to result in significant phase separation during air-cooling.

Water quenching from the carbide stabilisation treatment results in similar hardness, independent of the starting condition, corresponding to the hardness level observed after solution treatment and water quenching. This indicates that all prior cooling-induced γ' is dissolved at 1010 °C. Air-cooling from 1010 °C, however, results in significant differences between the mill-annealed and the solution-treated starting condition, where specimens

subjected to an initial solution treatment have hardness of approx. 20 HV higher. As the specimens showed very similar hardness after water quenching from carbide stabilisation, this difference must arise from differences in precipitation during cooling, which indicates that this process is affected by the prior solution treatment.

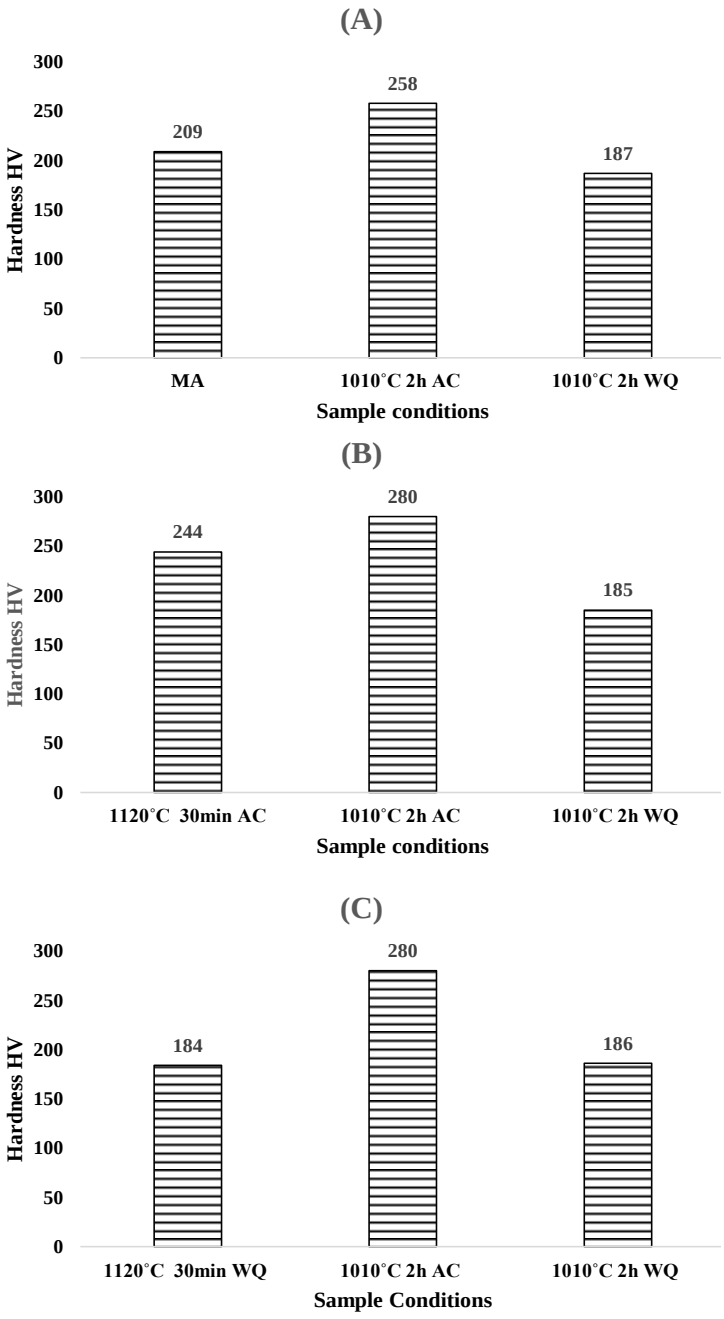

Figure 20 Hardness after different heat treatments as indicated in the chart in Figure. 17

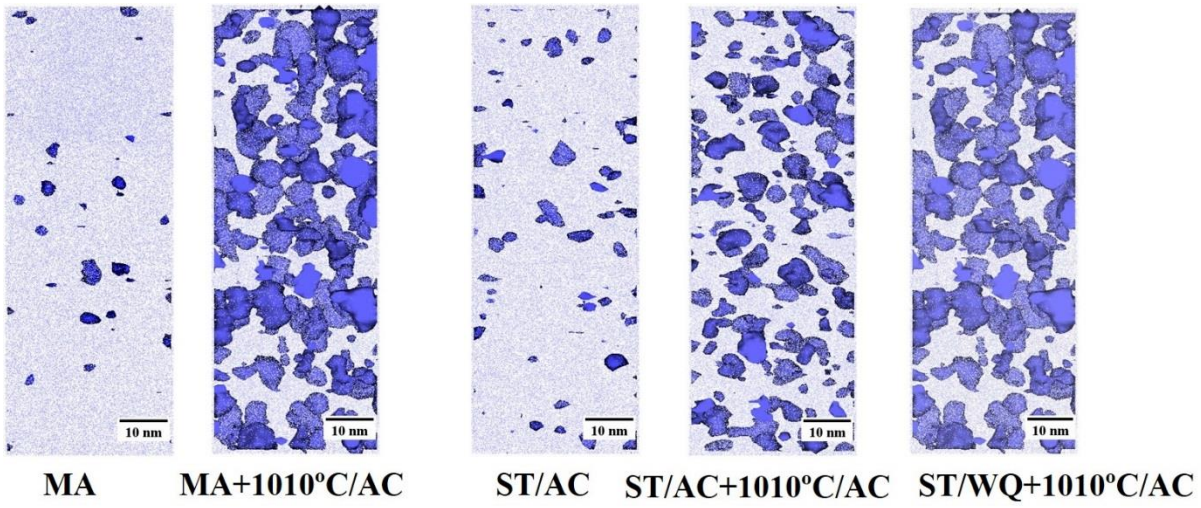

Figure 21 Atom probe tomography reconstructions of different material conditions, which indicate the presence of γ′ precipitates. A 7.5 at. % Al iso-concentration surface is used to visualise the γ/γ′ interfaces, with Cr atoms in light blue. The slice thickness is 35 nm.

The presence of γ′ in the mill-annealed state was confirmed by APT (Figure 20 and Table 10). Water quenching after solution treatment resulted in the complete absence of γ′, confirming the reason for the strength difference suggested above, whereas air-cooling produced a precipitation state qualitatively similar to the mill-annealed condition (Figure 20). The average γ′ size was the same in these two conditions (diameter 2.5 nm), whereas the number density is higher in the air-cooled solution treated specimen, which is consistent with the higher hardness.

Table 10 Results of APT analysis showing the size, number density and volume fraction of γ′ precipitates.

Starting condition	**Sample Identification**	**Hardness (HV)**	**Average diameter (nm)**	**Number density (nm^{-3})**	**Volume fraction (%)**
(A)	MA	209	2.5	0.00017	0.2
	1010 ˚C 2 h AC	258	6.0	0.00043	7.3
	1010 ˚C 2 h WQ	187	–	–	–
(B)	1120 ˚C 30 min AC	244	2.5	0.00033	0.3
	1010 ˚C 2 h AC	280	3.9	0.0011	5.8
	1010 ˚C 2 h WQ	185	–	–	–
(C)	1120 ˚C 30 min WQ	184	–	–	–
	1010 ˚C 2 h AC	280	4.2	0.0012	5.8
	1010 ˚C 2 h WQ	186	–	–	–

In the solution-treated and water-quenched material, water quenching from 1010 °C also resulted in no γ′ in the specimen. Air-cooling from 1010 °C, however, resulted in precipitation of γ′, consistent with the increased hardness in this material. The size and number density of the γ′ found after the carbide stabilisation treatment of the two-solution treated starting conditions are very similar. Absence of γ′ after carbide stabilisation and water quenching indicates that the particles were completely dissolved at 1010 °C, as the temperature histories during air-cooling from 1120 °C and 1010 °C were almost identical. The γ′ size after the 1010 °C treatment is larger (~4 nm compared to 2.5 nm) and the number density is higher by a factor of 3–4. The carbide stabilisation step applied after solution treatment clearly has a pronounced effect on the γ′ precipitation during the subsequent cooling. This effect is not related to the γ′ precipitated during the cooling from the initial solution treatment, as indicated by the similarity in the γ′ size and number density after air-cooling of the two solution treated conditions from 1010 °C, which again is consistent with the complete dissolution of γ′ at this temperature, as shown above.

It is also seen from the microstructure observed after carbide stabilisation and air-cooling of the mill-annealed starting condition, that the γ′ size is even larger (around 6 nm in diameter), but the number density is close to that observed in the mill-annealed or solution-treated and air-cooled condition. This significant difference from that observed after the 1010 °C treatment of the solution-treated starting condition confirms the pronounced effect of solution treatment on subsequent heat treatments.

5.3.2 Isothermal transformations

5.3.2.1 Gamma Prime

The phase transformation of γ′ precipitates is studied by microscopy analysis and hardness measurements. Results from the microscopy analysis, show that γ′ is precipitated as uniformly distributed spherical particles. With increasing ageing time, the particles increase in size from approximately 20 nm to 200 nm at 950˚C. Figure 22 a-f shows the distribution of γ′ in different aged samples at 950 ºC. In these micrographs it is clearly seen that there is a change in γ′ size and distribution at a given temperature of 950 ºC. At a higher ageing temperature than 950 ºC and ageing time of 26 h the particles tends to show no morphological change as seen in Figure 22f. γ′precipitation is also seen at grain boundaries at all the ageing temperatures and times.

With increasing ageing temperature, the particle size increases and their number density decrease which results in a decrease in hardness, as illustrated in Figure 23(b). γ′precipitates during higher ageing temperatures increase their size following a kinetic law described by the classical Lifschitz-Slyozov-Wagner theory (LSW) which prescribes a coarsening kinetics of γ′ phase precipitates as proportional to the cube root of ageing time [99-103]. It can be seen from

Figure 23(a) that the results are in good agreement with the LSW theory, because the proportionality of the size of the γ′ particles to the cube root of the ageing time is followed in all the reported temperature ranges.

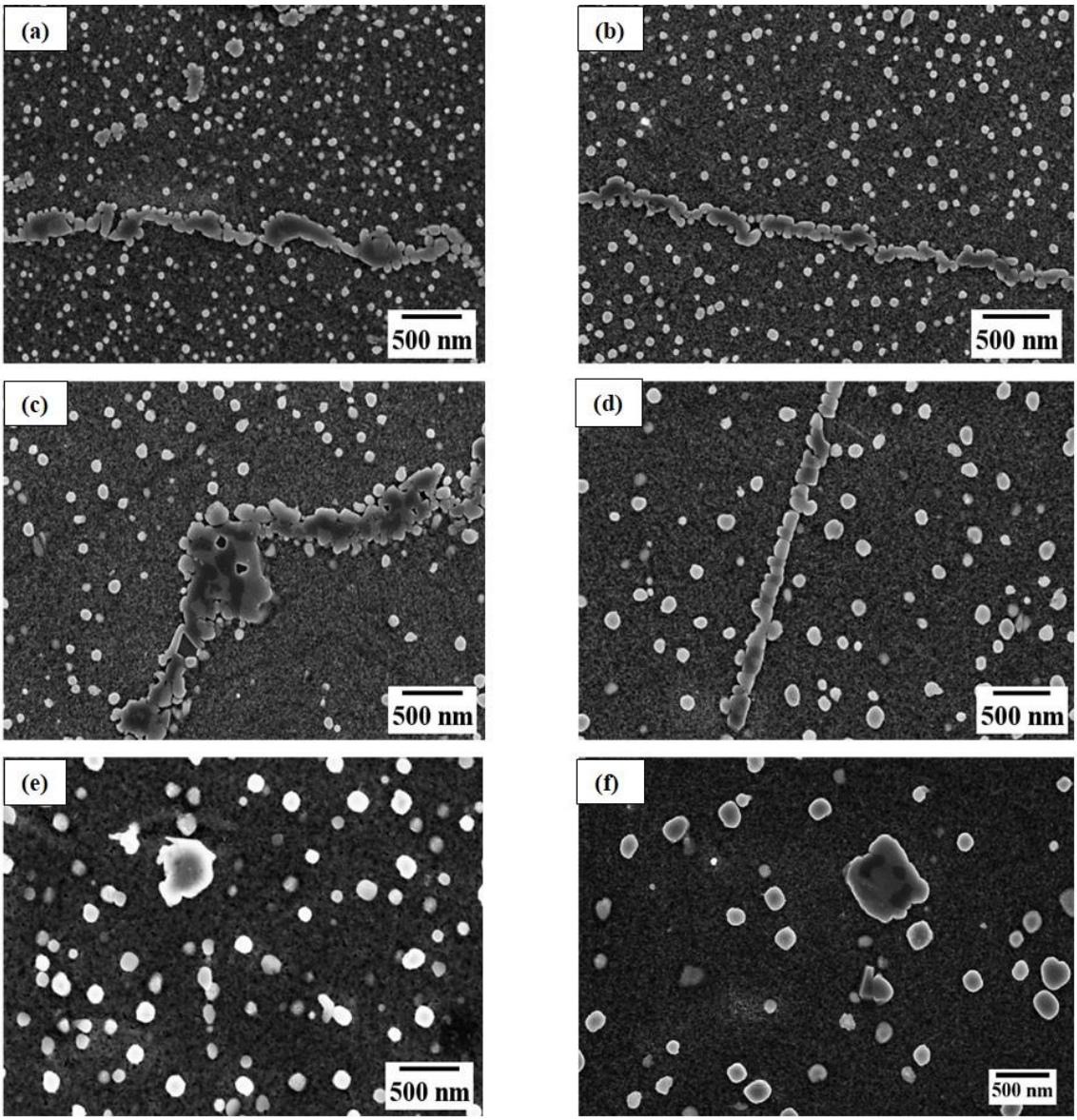

Figure 22 SEM images showing the growth of γ' precipitates with time at 950 ˚C. a) 30 min b) 1 h c) 2 h d) 5h e) 8 h and f) 26 h

It was also noted that the morphology of the γ′ precipitates was spherical at an ageing time of up to 98 h below 850 ºC. A similar trend was observed for all the ageing temperatures and ageing times in this study.

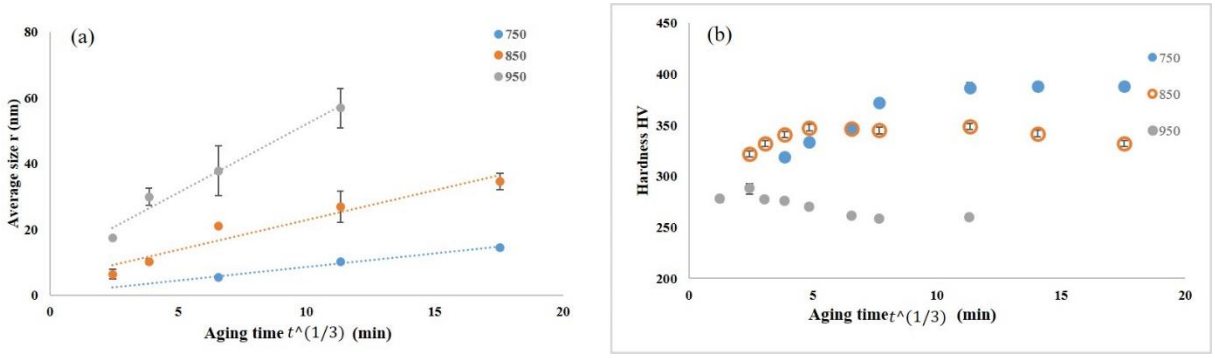

Figure 23 a) Size of γ'precipitates as a function of ageing time and b) hardness as a function of ageing time, at 750 ˚C, 850 ˚C and 950 ˚C.

Figure 24 shows the precipitation of γ′ at an ageing temperature of 1010 ºC after 1 hr. There are very few γ′ precipitates at this temperature but they are large. The γ′ solvus for Haynes 282 is reported to be approx. 997 ºC [1], but the presence of γ′ at 1010 ºC indicates that the solvus is well above 997 ºC.

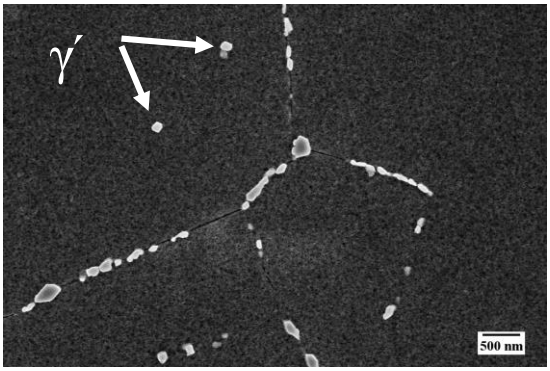

Figure 24 SEM image showing precipitation of γ′ at ageing temperature of 1010 ºC after 60 min

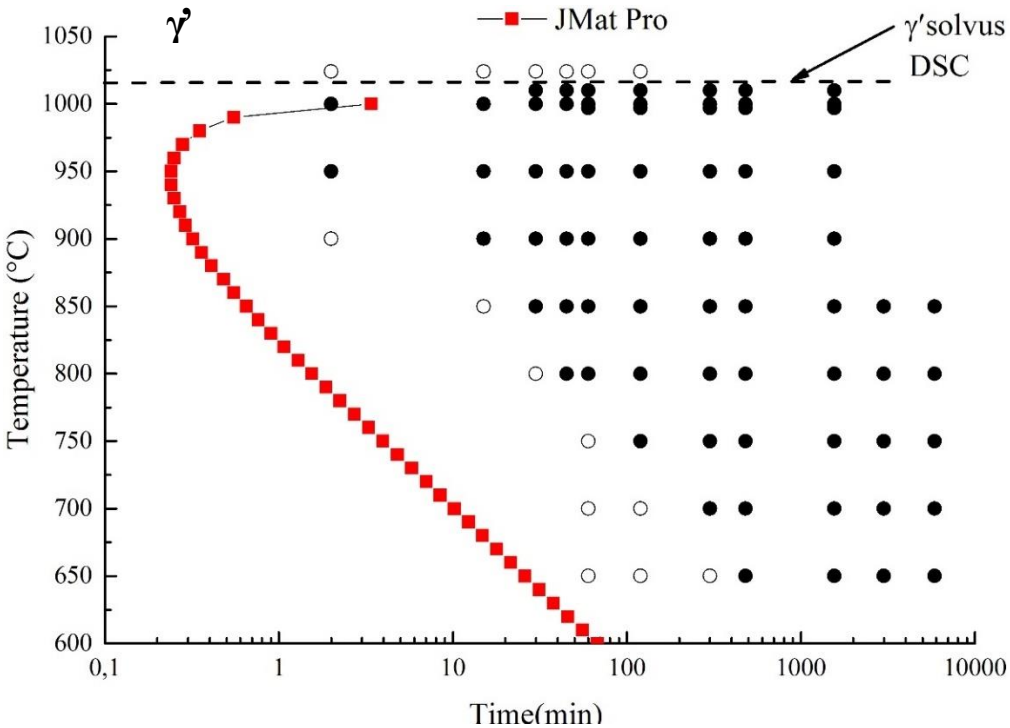

Figure 25 Experimentally determined γ′ under SEM as compared to JMatPro for Haynes 282

Figure 24 shows the observed γ′ under SEM for 1010 ºC after 60 min. This indicates that the γ′ solvus is above 1010 ºC. Figure 25 shows the presence of γ′ precipitates under SEM as compared to that predicted by JMatPro. The open circles indicate that γ′ precipitates are not detected. The SEM images for specimens at 1024 ºC showed no presence of γ′ precipitates whereas they are observed at 1010 ºC as shown in Figure 24. Hence the experimentally observed γ′ solvus is well above 1010 ºC but below 1024 ºC, which corresponds to that observed through JMatPro analysis but is slightly higher than that reported in literature [1].

5.3.2.2 Carbides

In Haynes 282 carbides such as MC, $M_{23}C_6$ and M_6C are present. The two types of MC precipitates found in the Haynes 282 alloy; Ti-rich nitride and Ti-Mo-rich carbide precipitated both inter and intragranularly. These carbides are generally characterised as having a coarse, random, blocky morphology that was found to be stable over the ageing temperature ranges in this study. M_6C and $M_{23}C_6$ carbides are formed as series of separate discrete grain boundary particles, but the morphological separation of these grain boundary carbides proved difficult. .

Figure 26 a-f shows micrographs of samples at different ageing temperatures for an ageing time of 2 h. At higher temperatures the morphology of the carbides changes from a film-like appearance at lower temperatures to brick morphology, and finally to discrete morphology at higher ageing temperatures. At much higher aging and solutionising temperatures above 1100 ^{o}C, the grain boundary carbides dissolve completely and appear free from carbides. At temperatures below 750 ˚C the carbides appear as a continuous film in the grain boundaries. Such films can reduce the ductility and impact strength of material [57, 101]. At a particular ageing temperature, with increasing ageing times as shown in Figure 27 there is no change in grain boundary carbide morphology.

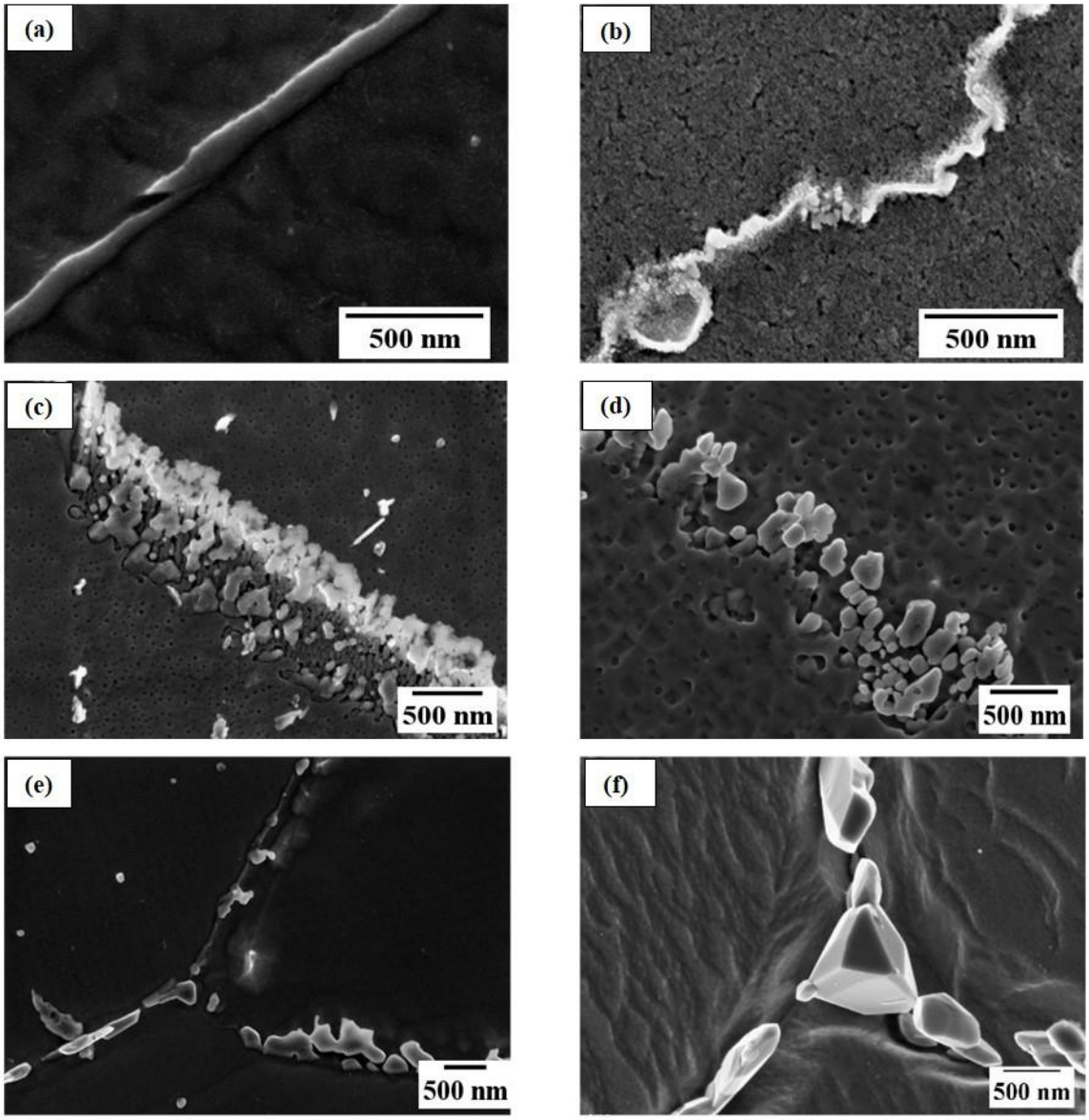

Figure 26 SEM images showing the morphological changes in the grain boundary carbides with variation in temperatures at 2 h a) 650 ˚C b) 750 ˚C c) 850 ˚C d) 950 ˚C e) 1000 ˚C f) 1050 ˚C.

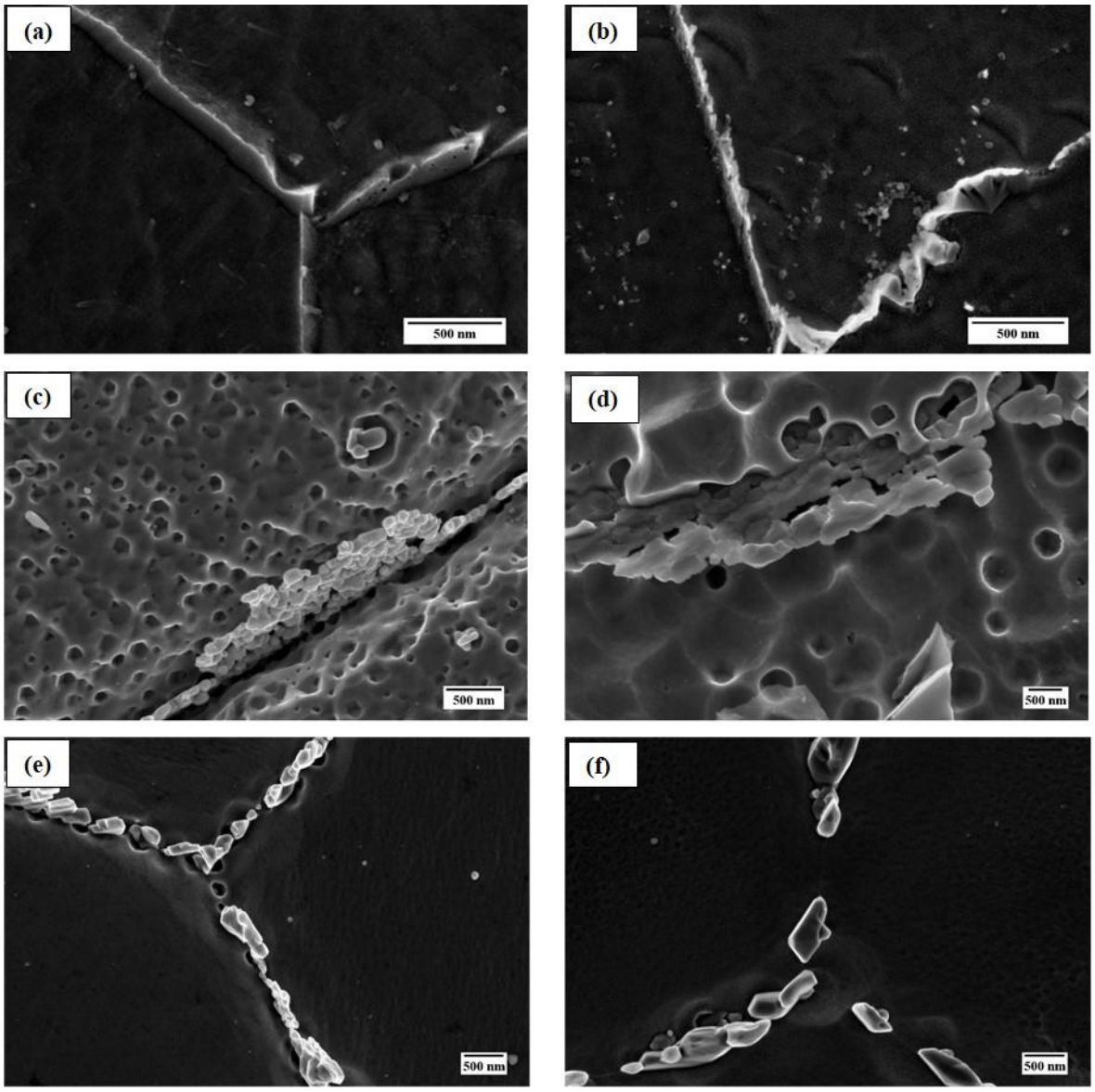

Figure 27 SEM images show that there are no morphological changes in the grain boundary carbides with an ageing time at (a) 650 ˚C and 30 min (film morphology) (b) 50 h and 950 ˚C (brick morphology) (c) 2 h (d)26 h and 1000 ˚C (discrete morphology) (e) 2 h and (f) 26h

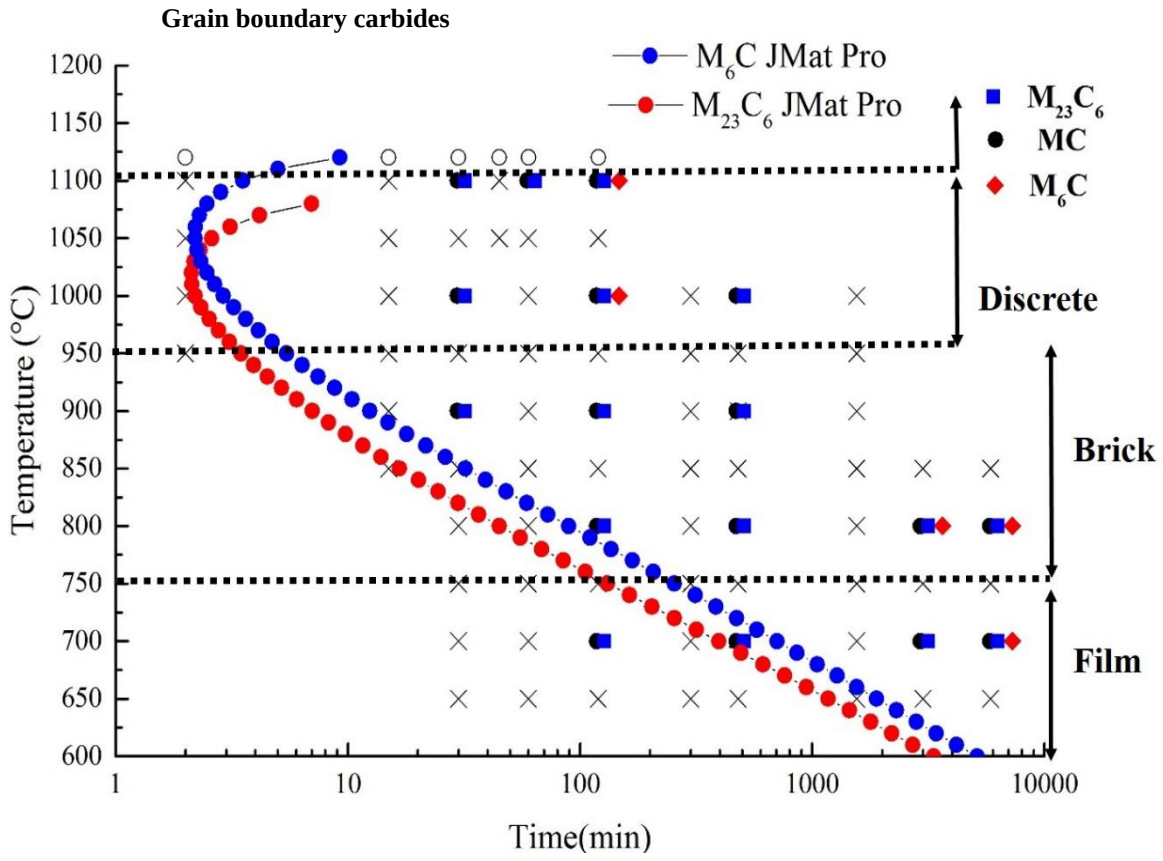

x: carbides are observed but are not identified by EDX

o grain boundary carbides are not present

Figure 28JmatPro phase transformation for M_6C and $M_{23}C_6$ carbides and presence of experimentally determined grain boundary carbides during isothermal phase transformation

Figure 28 contains a summary of the experimental observations for the carbides. Also included are the curves for $M_{23}C_6$ and M_6C obtained from the JMatPro simulations. The simulated TTT curves were calculated using the equilibrium composition of the γ matrix obtained from equilibrium calculations at 1150 °C. The upper temperature limit for both $M_{23}C_6$ (around 1100 °C) corresponds with the experimental observation, whereas the upper limit prediction for M_6C is far too high. For M_6C, the experiments show complete dissolution of grain boundary carbides above 1100 °C, but rapid precipitation is predicted to occur even up to approx. 1150 °C. Furthermore, when comparing the experimental solvus temperature of $M_{23}C_6$ (approx. 1100 °C) with the predicted equilibrium phase calculations in Figure 15, it is seen that the solvus limit is under-predicted by JMatPro (it is approx. 850 °C). Here it must also be noted that there is contradiction between the equilibrium calculation and the predicted carbide precipitation simulation, as the latter predicts $M_{23}C_6$ formation at temperatures of up to almost 1100 °C, 250 °C above the predicted equilibrium solvus temperature.

5.4 Sensitivity to heat treatment

In order to study the sensitivity of Haynes 282 to heat treatment temperatures and to understand its subsequent impact on room temperature properties, the heat treatment schedules as shown in Table 4 were done on mill-annealed specimens.

After heat treatment, the carbide morphologies at the grain boundaries changed. Figure 29 shows the different morphologies of grain boundary carbides. Figure 29(a) shows the occasional presence of discrete grain boundary carbides in as-received condition. With additional solutionising followed by conventional heat treatment (ST+A), the grain boundary shows interconnected morphology (Figure 29(b)). In MA+A condition, however, grain boundary carbides have discrete morphology (Figure 29(c). However, unlike ST+A and MA+A conditions, MA+LTA shows discrete grain boundary carbides and γ′ precipitates (Figure 29(d)).

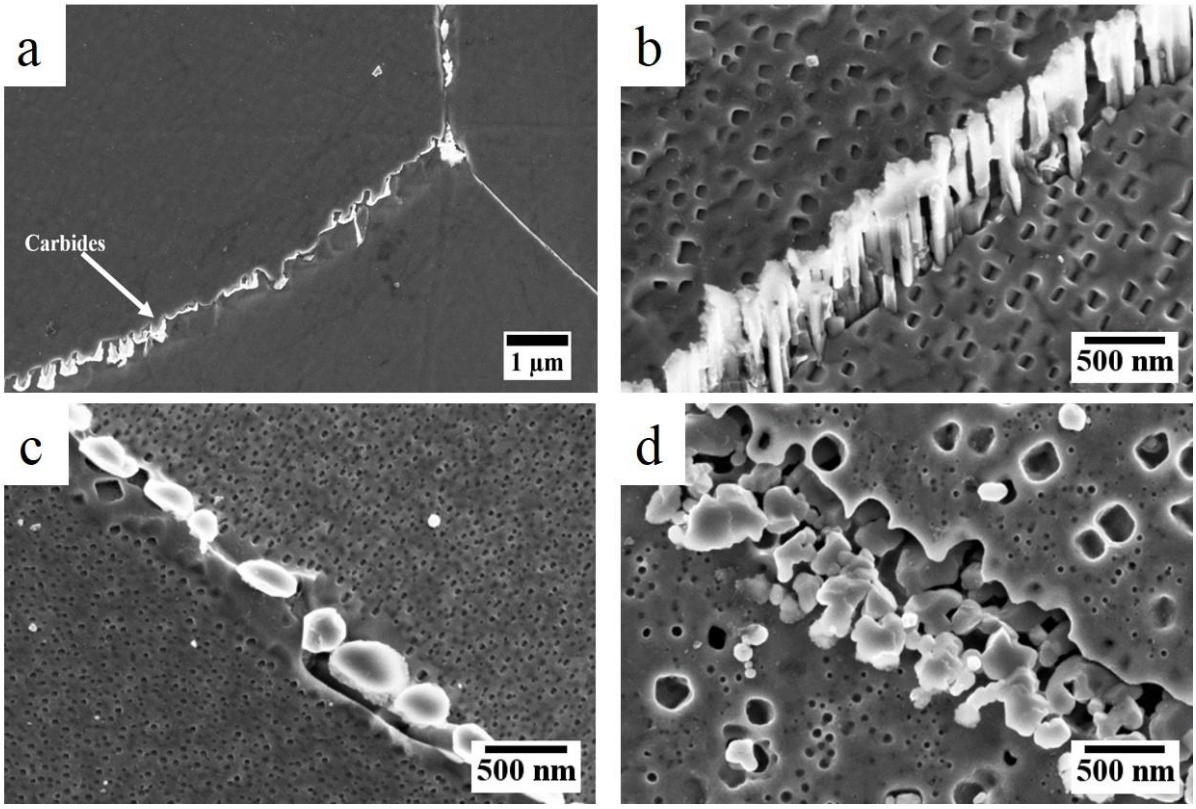

Figure 29 Showing differences in carbide morphologies at the grain boundaries in different conditions (a) Carbides in as-received condition: occasional presence of discrete grain boundary carbides (b) ST+A condition: presence of interconnected grain boundary carbides (c) MA+A condition: discrete grain boundary carbides (d) MA+LTA condition: discrete grain boundary carbides and coarse γ′ precipitates.

Furthermore, γ′ etching also showed morphological changes, as seen in Figure 30. Figure 30(a) shows no presence of γ′ in as-received condition. In ST+A, i.e. additional solutionising followed

by conventional heat treatment, γ′ precipitates are seen with cuboidal morphology (Figure 30(b)). While, MA+A shows the presence of fine spherical γ′, (Figure 30(c). However, unlike other conditions, MA+LTA shows bimodal γ′ precipitates (Figure 30(d)) with spherical and cuboidal morphology.

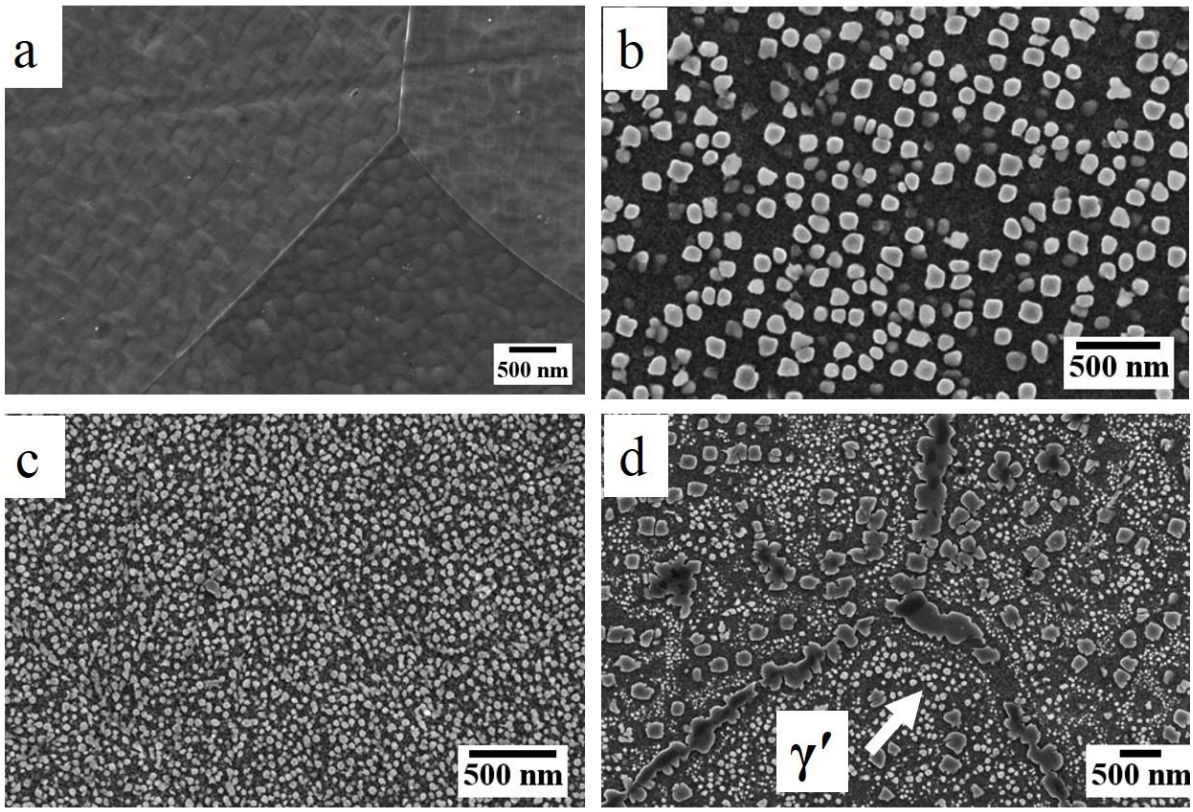

Figure 30 SEM images showing differences in carbide morphologies at the grain boundaries in 4 different conditions (a) As-received condition: No γ′ seen (b) ST+A condition: cuboidal γ′ (c) MA+A condition: spherical γ′ (d) MA+LTA condition: bimodal γ′ precipitates (small-spherical and coarse-cuboidal).

The morphological changes in grain boundary carbides and γ′ precipitates were tested for their impact on room temperature tensile properties and hardness. The tensile test results as well as hardness and morphological changes in γ′ are summarised in Table 11.

Table 11 Tensile test results showing impact on room temperature properties and hardness for different heat-treated conditions.

Heat treatment condition	**Room temperature**				**Hardness (HV)**	**γ´ morphology**
	0.2% YS(MPa)	**UTS(MPa)**	**% El**	**%RA**		
As-received					212 ± 4	
ST+A	650	1100±10	16± 1	14	310 ± 6	Cubic (120nm)
MA+A	760±8	1245±10	32± 1	33	358 ± 8	Spherical (20-30nm)
MA+LTA	765±8	1255±10	32± 1	34	327 ± 6	Bimodal (cubic + spherical) (120nm+ 20nm)

As seen in Table 11, the strength in ST+A condition is lower compared to other heat treatments. From literature it is evident that γ′ precipitation strengthens the material. A change in the size of γ′ precipitates to coarse cuboidal morphology of 120 nm affects its room temperature YS and UTS. However, in MA+A- and MA+LTA- conditions, strength levels are similar.

Elongation is affected in ST+A condition and can be considered to be the effect of the interconnected morphology of carbides at grain boundaries. The discrete carbide morphology does not affect the tensile ductility in MA+A and MA+LTA conditions, which is consistent with observations reported in literature. Hardness values are high for MA+A condition with fine spherical γ′ compared to the coarse cuboidal precipitates in ST+A condition. However, the bimodal precipitate morphology for MA+LTA shows hardness in between the two conditions.

This study shows that solution heat treatment not only changes the γ′ morphology but also affects the grain boundary morphology which has a direct impact on the room temperature strength and elongation properties. Furthermore, carbide stabilisation at a lower temperature also showed bimodal γ´ distribution. This creates a need for systematic understanding of the influence of heat treatment parameters on the microstructure and properties of this alloy.

5.4.1 Variation in heat treatment parameters

5.4.1.1 Variation in solution treatment parameters

In order to study the influence of solution treatment parameters, a systematic microstructural study was carried out as shown in Table 5. The hardness measurement on these heat-treated specimens showed that the cooling rate influences the hardness of the material after solution treatment as shown in Figure 31(a). At a slow cooling rate such as air–cooling, hardness

increases by 60 HV compared to a measurement of 180 HV for the water-quenched specimens. However, hardness after the standard two-step ageing is similar, as seen in Figure 31(b).

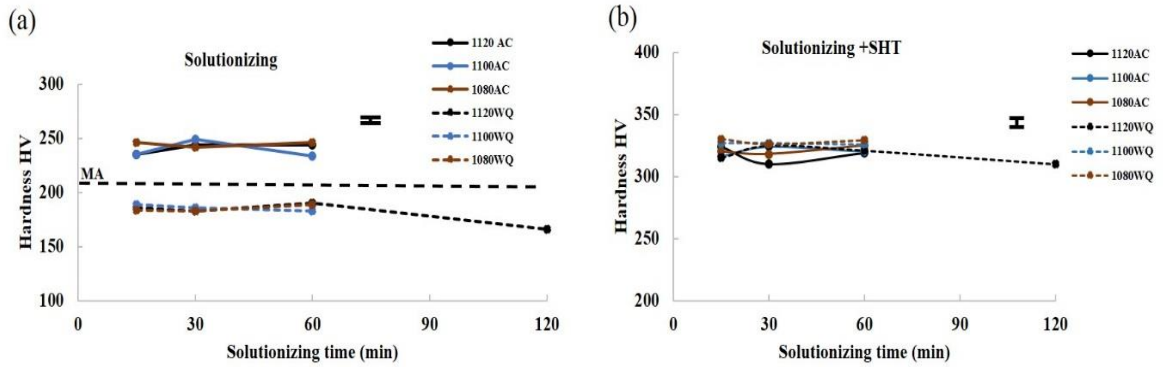

*SHT: 1010 ˚C -2 hr AC+788 ˚C-8hr AC

Figure 31 Measured Hardness on samples (a) After solution treatment (b) Solution treatment and SHT

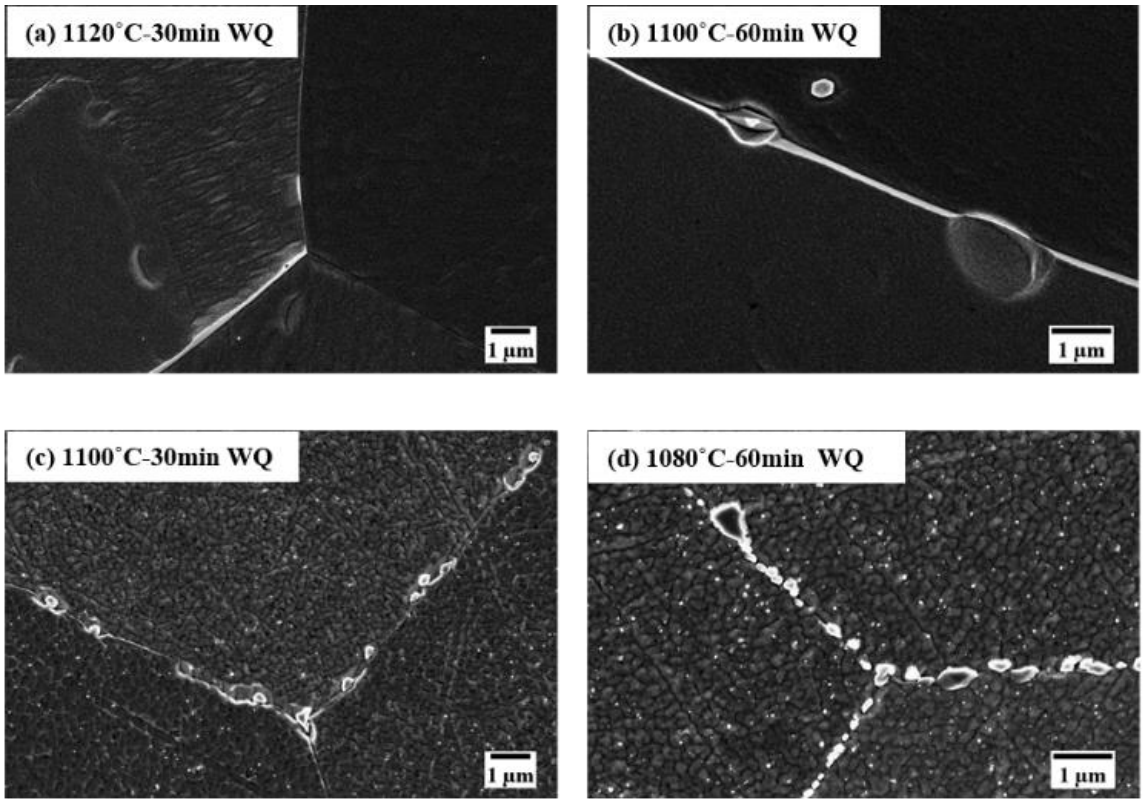

(*WQ: Water quench)

Figure 32 SEM micrographs of Haynes 282 solution-treated and water-quenched for different temperatures and times showing absence of grain boundary carbides in conditions (a) - (b) and presence of carbides in conditions (c)-(d).

Figure 32 shows the SEM micrographs of Haynes 282 after solution treatment. Solution treatment at 1120 ºC for 30 min, and 1100 ºC for 60min were sufficient for complete

solutionising without grain growth as no grain boundary carbides were observed under SEM (Figure 32 a-b). As seen in Figure 32 c-d, low temperature solution treatment at 1080 ºC and 1100 ºC for 30 min were insufficient, as the presence of grain boundary carbides was observed. Furthermore, solution treatment at 1120 ºC for 2 h showed a drop-in hardness after solution treatment (Figure 31a), but grain growth was not observed in this case. However, abnormal growth of some grains was observed.

Figure 33 shows the morphology of γ′ precipitates after full heat treatment. As seen here, γ′ precipitates are unimodal and uniformly distributed in the matrix and did not show any changes on ageing from the initial variations in solution treatment conditions.

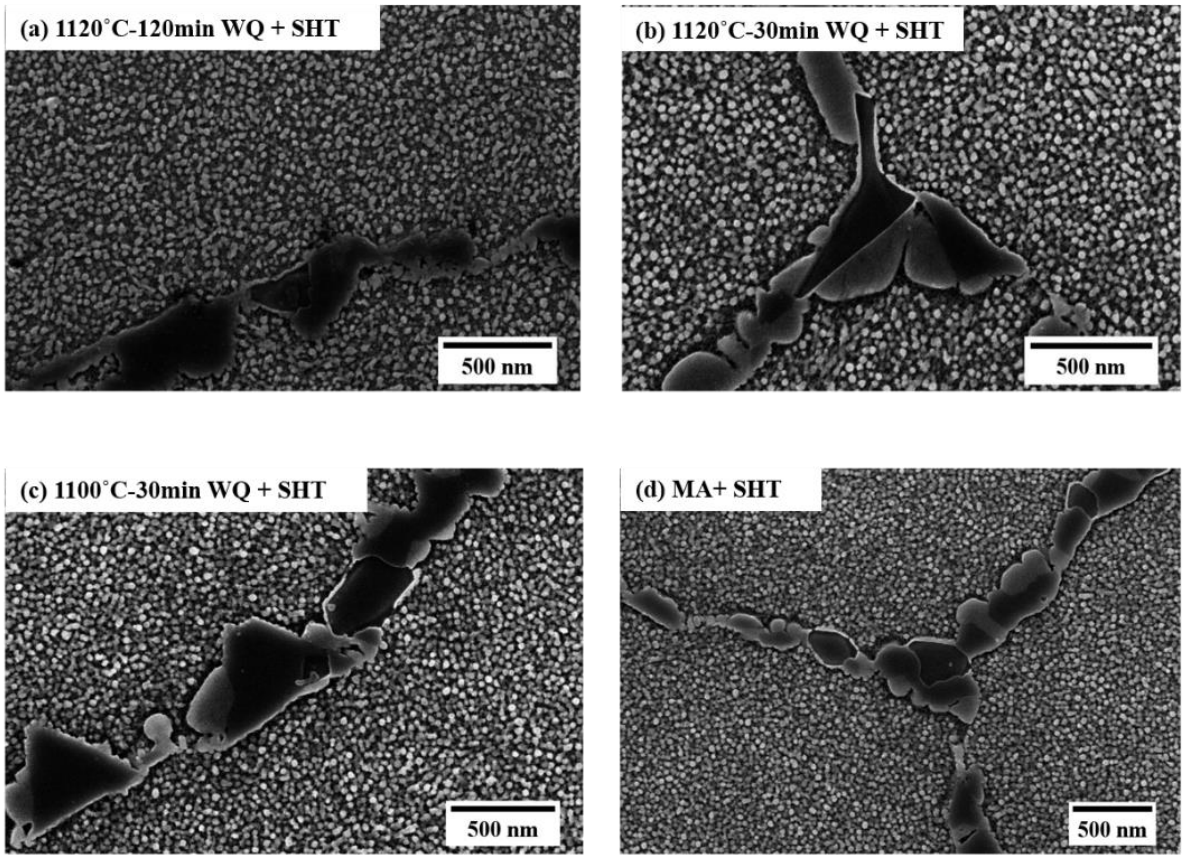

*SHT: 1010˚C -2h AC+788˚C-8h AC * MA: Mill annealed (No solution treatment)

Figure 33 SEM micrographs of Haynes 282 showing γ′ precipitates after standard two-step ageing

Based on these observations, a set of heat treatment parameters as shown in Table 6 were performed in order to understand the effect of these parameter variations on tensile properties both at room temperature and high temperature.

The mechanical properties of the heat-treated specimens according to Table 6 are shown in Figure 34. As seen here the mechanical strength at room and high temperature is unaffected by variations in solution treatment variations. The strength at room temperature was higher than at

high temperature. The strength properties are dependent primarily on the γ′ precipitates and, as seen in Figure 23, the morphology and size of these precipitates are similar due to the standard two-step ageing. Therefore, no change has been observed on the strength properties. However, there are slight variations in ductility, as seen in Figure 34(c). Ductility at room temperature was higher than at high temperature except for two conditions at 1120 ºC 30 min WQ and AC. This change in ductility could be due to differences in the size, distribution and amount of grain boundary carbides as seen in Figure 35.

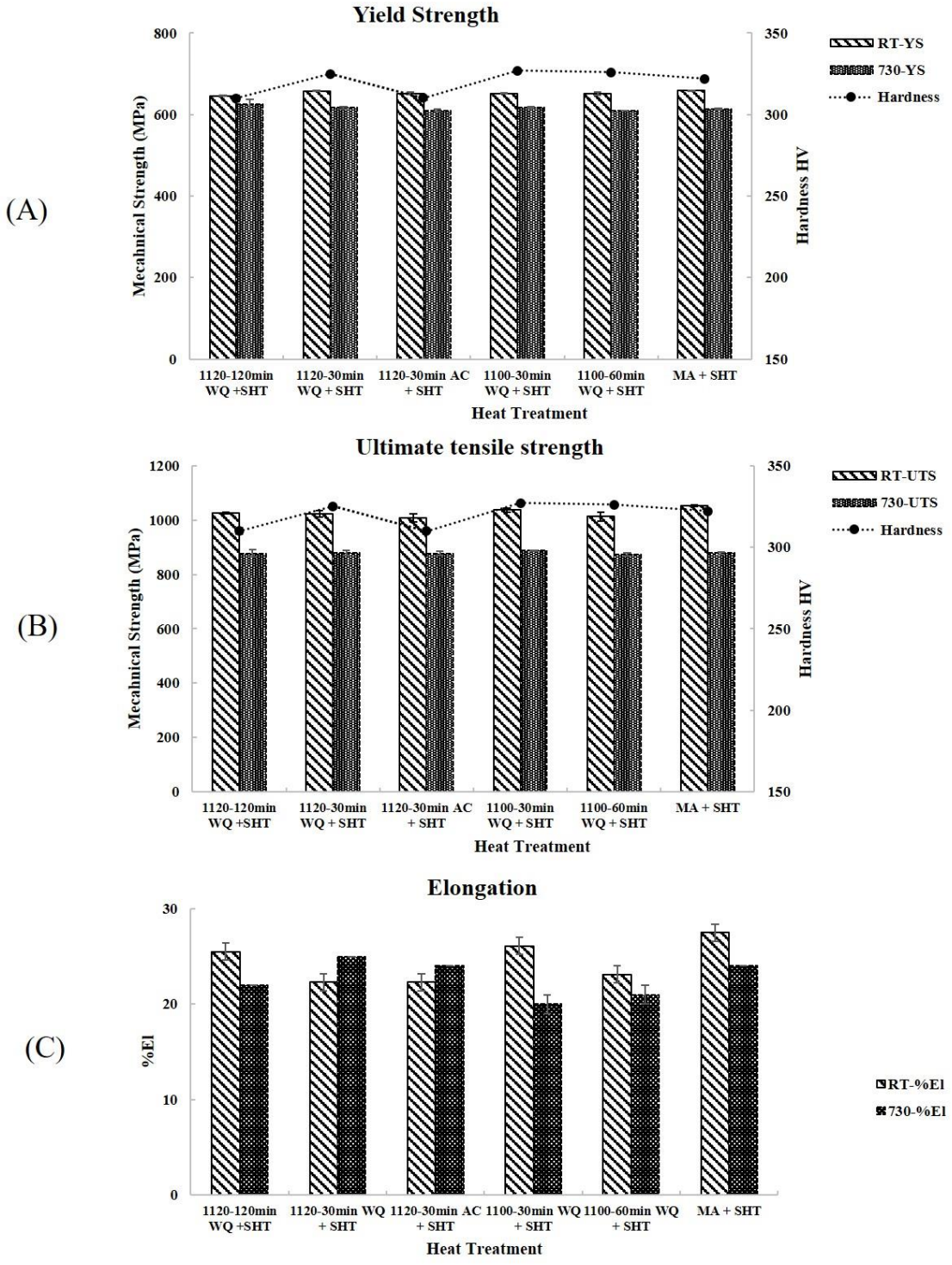

Figure 34 Mechanical properties at 25 and 730 ˚C for all the heat-treated conditions in Table 6 (a) Yield strength (b) Ultimate tensile strength (c) Elongation.

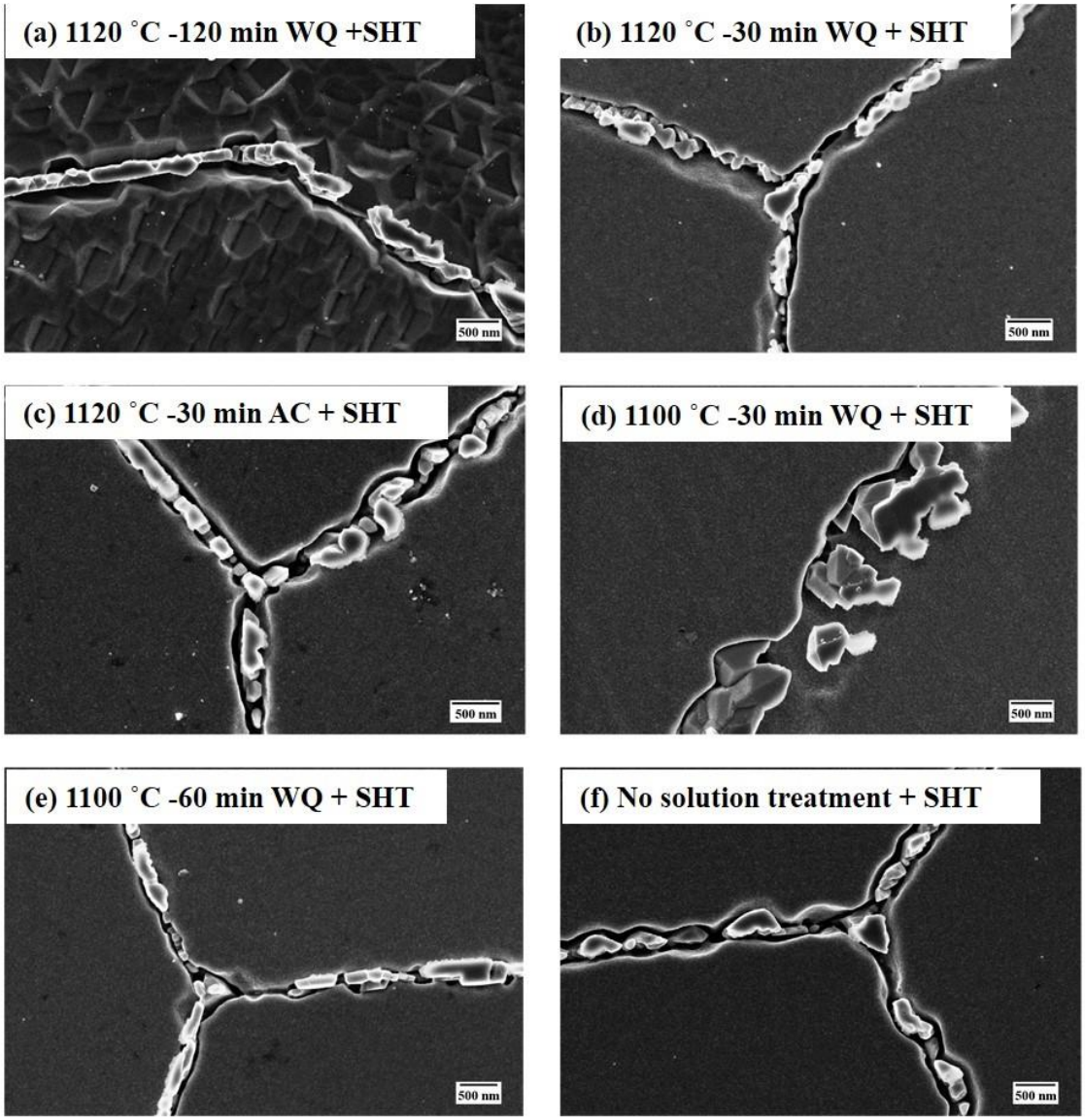

Figure 35 SEM micrographs of Haynes 282 for different heat treatment conditions as in Table 3 showing grain boundary carbides after the full heat treatment.

It can also be seen that Haynes 282 on direct ageing has better properties at room and high temperature compared to having an additional solution treatment, and therefore solution treatment might not be required.

5.4.1.2 Variation in carbide stabilisation parameters

In order to understand the influence of carbide stabilisation parameter variations on microstructure, heat treatment trials were performed for conditions as shown in Table 7. From the microstructural and hardness measurement it is seen that the carbide stabilisation step affects the morphology of grain boundary carbides depending on the initial state of the material. As seen in Figure 36 the carbide morphology is different in all three conditions. The morphology of the grain boundary carbides is discrete in MA condition but brickwall in solutionised states (Figure 36 b and c).

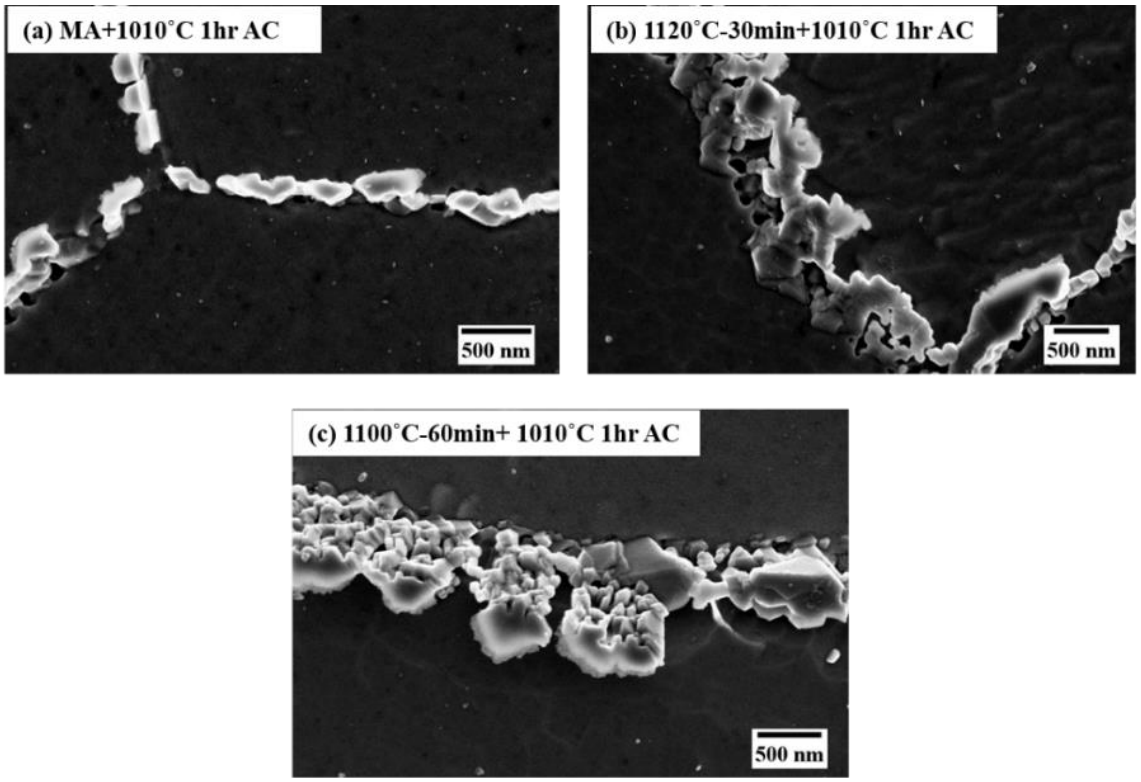

Figure 36 SEM micrographs showing the carbide morphology at grain boundary after 1010 ˚C for 1 h AC condition for specimens in three different initial states (a) MA (b) 1120 ˚C 30 min WQ (c) 1100 ˚C 60 min WQ

However, this change does not appear to affect the hardness of the material after carbide stabilisation or after ageing. The temperature variation is seen to affect not only the γ′ morphology but also the carbide morphology. A similar behaviour is observed with variations in cooling rate. Furthermore, a slow cooling rate such as furnace cooling results in bimodal γ′ precipitation. The influence of carbide stabilisation parameter variations on mechanical properties was studied according to heat treatment conditions according to Table 8. The SEM micrographs showing the difference in grain boundary carbide and γ′ morphology are shown in Figures 37 and 38 respectively. As seen in Figure 37 the carbide morphology appears as discrete for the heat treated conditions at 1010 °C and 996 °C at both air-cooling and furnace cooling as seen in Figure 37 (a)-(d). However, on direct ageing, i.e. omitting the carbide stabilisation step, the carbide morphology is seen as a continuous film-like morphology (Figure 37 (e)-(f)).

As can be seen there is microstructural variation in terms of γ′ morphology observed after full treatment from (Figure 38 (a)-(d)), however no change was observed on direct ageing (Figure 38 e-f). On air-cooling at 1010 ºC the γ′ is unimodal with spherical morphology of 20 nm (Figure 38a), while on furnace cooling precipitation is bimodal with square and spherical morphology (Figure 38c). With a small drop in temperature of 14 ˚C, γ′ precipitation at 996 ˚C

is bimodal on both air-cooling and furnace cooling. On air-cooling the γ′ at 996 ˚C is spherical but in two different size classes (Figure 38 b) while on furnace cooling it appears square and spherical (Figure 38 d). On direct ageing the γ′ precipitation is more unimodal and spherical (Figure 38 e-f).

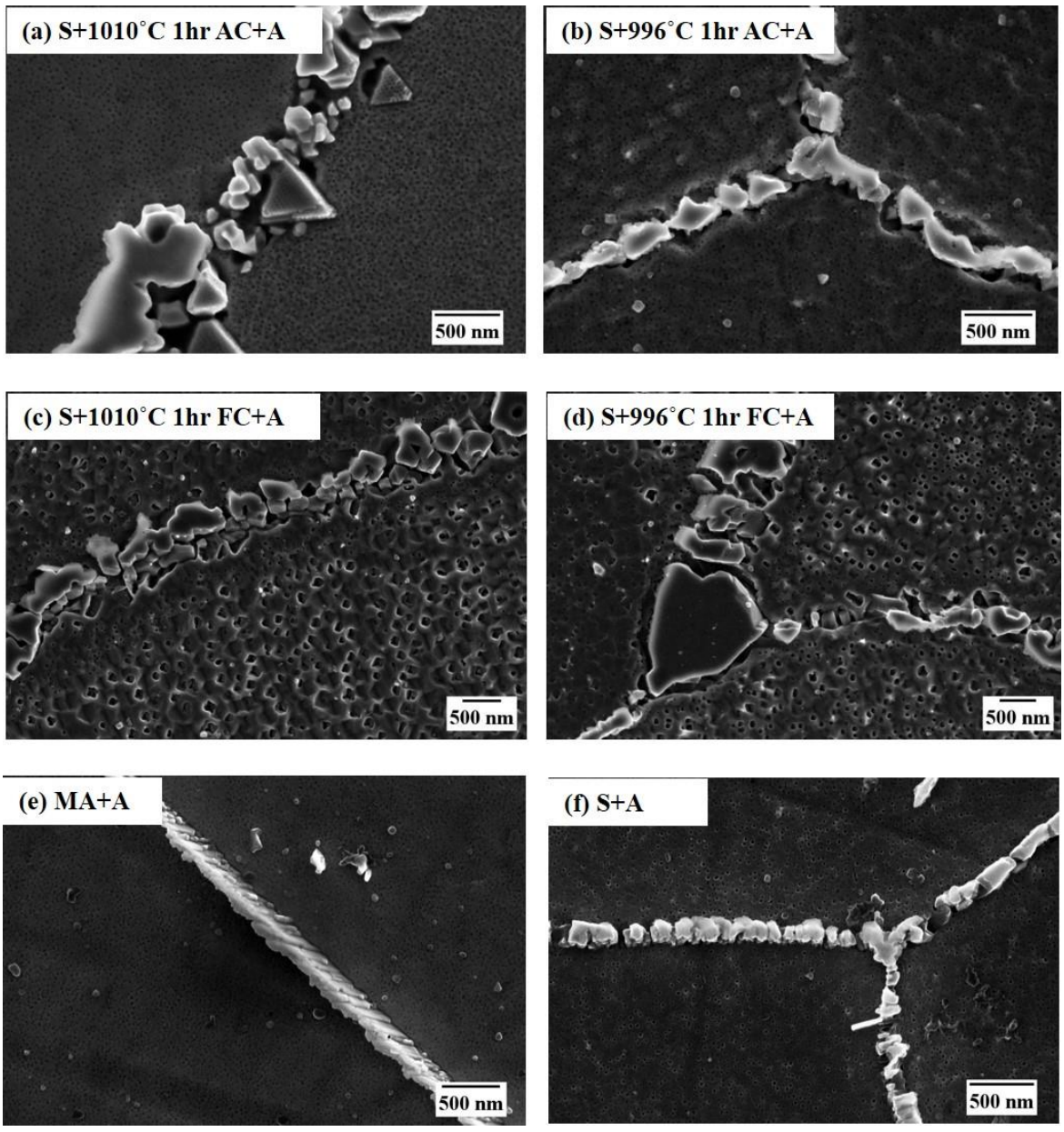

*S: 1100˚C-60min WQ A: 788˚C-8h AC

Figure 37 SEM micrographs showing the carbide morphology for 1100 ˚C 60 min WQ solutionised state for different carbide stabilisation conditions as in Table 8.

From the microstructural observation it can be concluded that variation in the carbide stabilisation temperature does not influence the carbide morphology but does affect the γ′ morphology. The cooling rate after carbide stabilisation affects the γ′ morphology while the effect on the carbide morphology is insignificant. On direct ageing, the carbide morphology

changes to a continuous interconnected morphology, however, its influence on γ′ is insignificant i.e. it shows unimodal distribution as seen in standard heat treatment. This means that the carbide stabilisation step is essential in order to obtain the desired grain boundary carbide morphology.

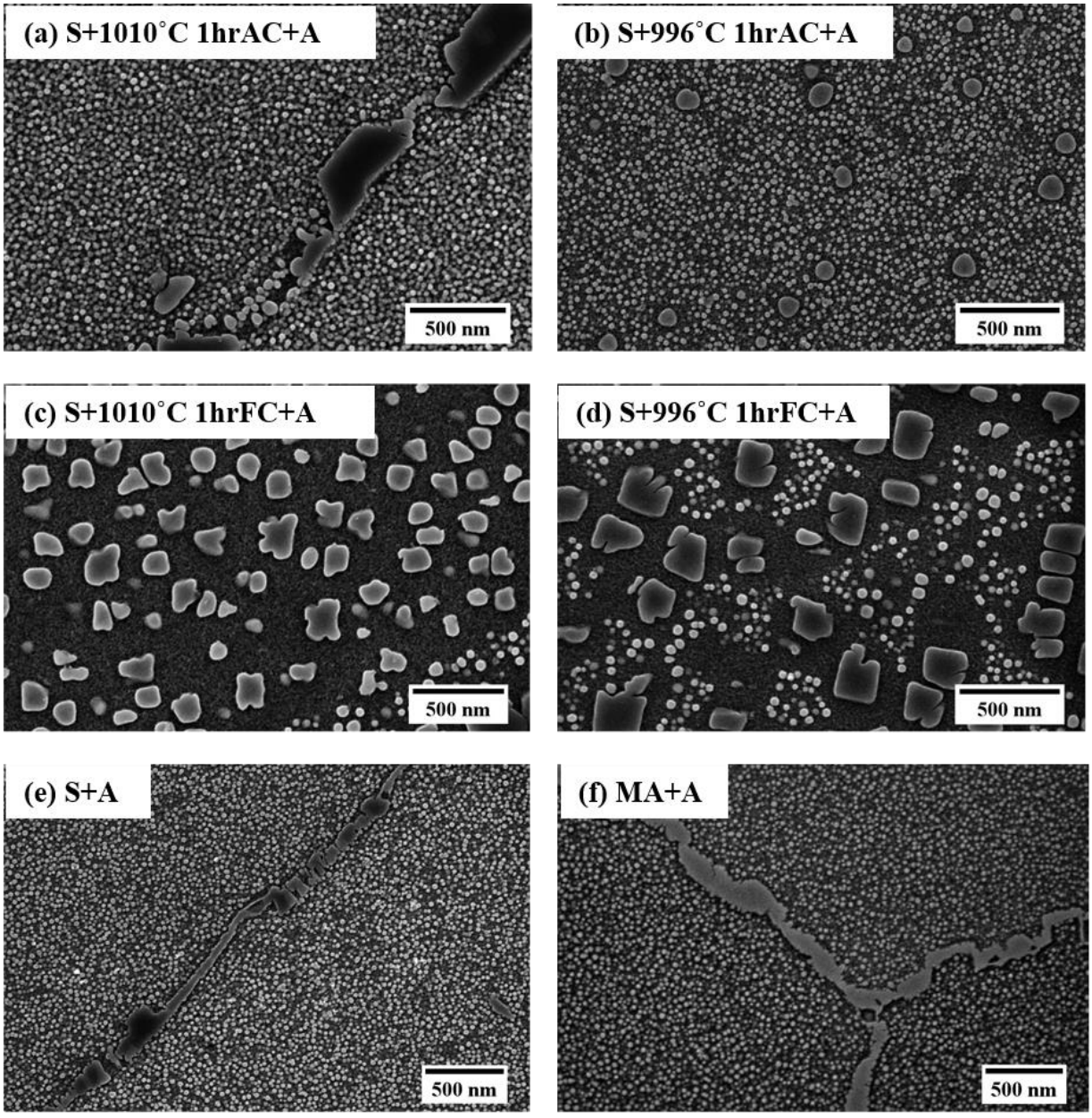

Figure 38 SEM micrographs showing the γ′ morphology for 1100 ˚C 60 min WQ solutionised state for different carbide stabilisation conditions as in Table 8.

In order to understand the influence of these microstructural changes on mechanical strength, tensile tests were performed on selected heat treatment as mentioned in Table 8. The results of mechanical tests both at room and high temperature, such as the yield strength (YS), ultimate tensile strength (UTS) and elongation (EL) for the heat treatment matrix shown in Table 8 are shown in Figure 39.

(A)

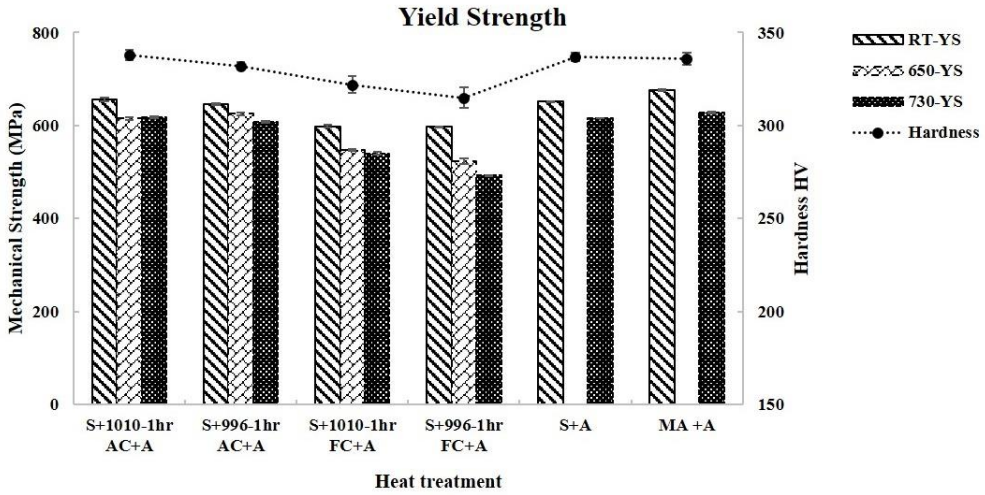

(B)

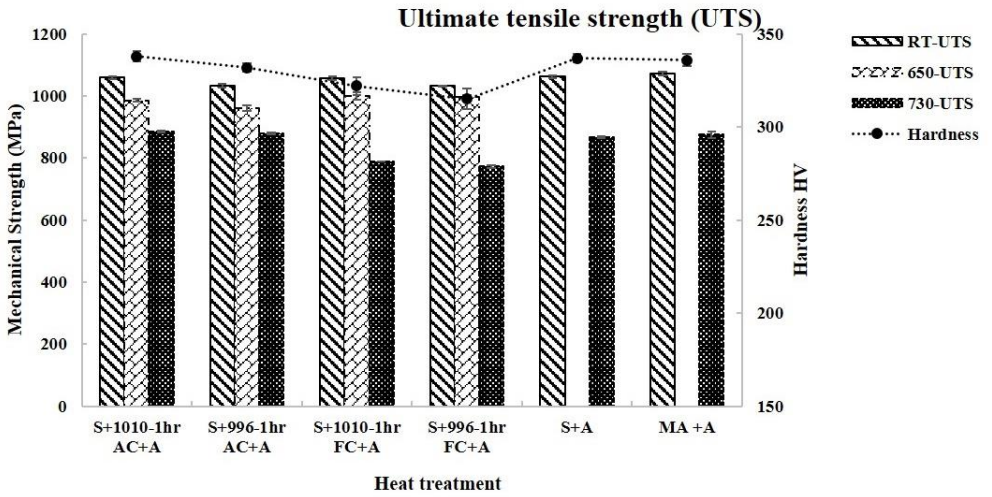

(C)

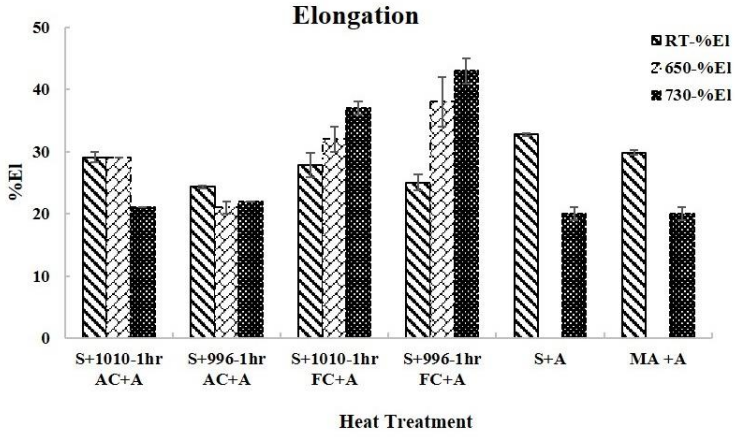

Figure 39 Mechanical properties at 25 and 730 ˚C for all the heat--treated conditions in Table (3) (a) Yield strength (b) Ultimate tensile strength (c) Elongation.

Tensile strength at room temperature is very similar for all conditions. Ductility at room temperature is slightly lower for the sub solvus-treated conditions, whereas the direct aged state showed higher ductility. The strength levels decrease with temperature for all conditions, and the decrease is greatest in the FC conditions. The YS at both 650 and 730 °C follows the same trend as at room temperature, with lower strength levels in the FC conditions, and similar values

are observed for AC and direct aged conditions. At 650 °C, all conditions exhibit similar UTS values, as in the case at room temperature. A difference can, however, be seen at 730 °C, where the FC conditions show lower UTS levels compared to AC and direct aged material.

The most drastic differences in behaviour occur in ductility at high temperature. Whereas the EL values decrease significantly in the AC and direct aged conditions at higher temperatures, the FC material shows a continuous increase in ductility with increasing temperature.

In short, the carbide stabilisation temperature, and the subsequent cooling rate, have pronounced effects on the tensile properties of Haynes 282. Slow cooling leads to lower yield strength and a more pronounced drop in strength at higher testing temperatures. The effects on UTS are similar, at least at high temperatures, but much less pronounced. The property which is most significantly affected is the ductility, which is lower after stabilisation at 996 °C compared to at 1010 °C at room temperature. At high temperatures, ductility after FC increases significantly with temperature, whereas there is a drastic drop in ductility for AC and direct aged conditions. Direct aged material behaves similarly to AC conditions in terms of both strength and ductility, although the reduction in ductility at high temperatures is more pronounced.

5.5 Anisotropic ductility

In the ductility study of forgings, mechanical tests on specimens from Haynes 282 forgings, showed similar values for YS, while their ductility and to some extent UTS changed. In this section, observations from representative samples are discussed. The fractography of tensile test specimens showed intergranular failure as shown in Figure 40. Figure 40(a), shows a sample with intergranular failure and Figure 40(b) with the presence of cracked MC carbide at the grain boundaries, and the presence of dimpled features on the fracture surface indicating a ductile matrix.

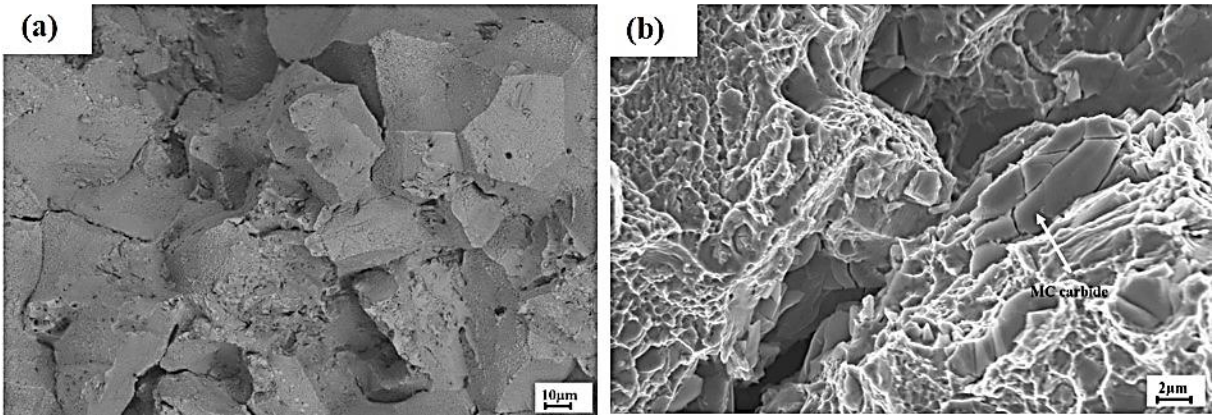

Figure 40 Fractographs of tensile specimen showing (a) Intergranular failure (b) Presence of dimpled features, intergranular failure and cracked MC carbide at the grain boundary

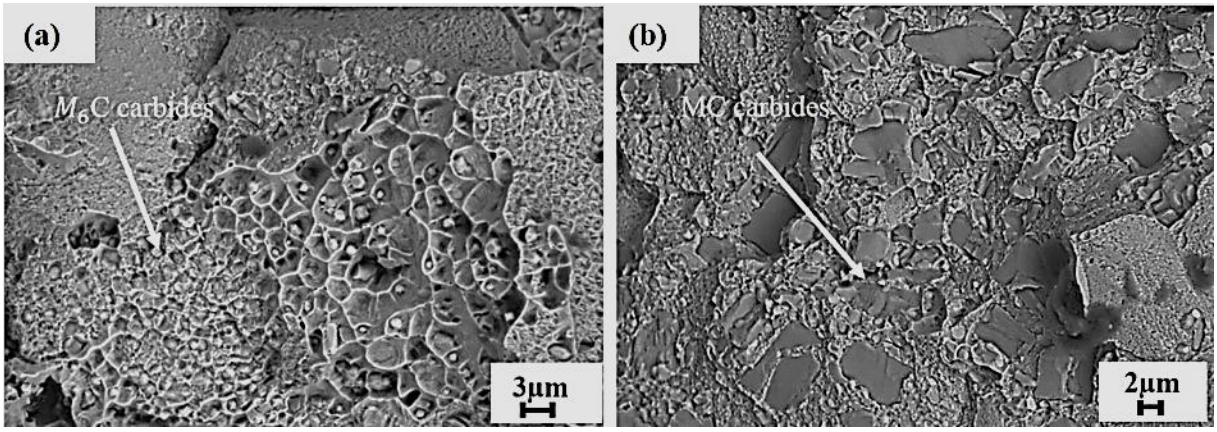

Figure 41 The fractography showing presence of segregation of (a) M6C carbides (b) MC carbides

Segregated M_6C and MC carbides were also present on the fracture surface as shown in Figure 41. In order to understand the segregation of carbides and their distribution, longitudinal sections of specimens were cut, polished and etched for microscopy. Figure 42 (a) shows the longitudinal section of a sample just below the fracture surface, indicating cracks along a segregated carbide region. A region with segregated carbides, shows the presence of M_6C, MC carbides and carbo-nitrides, as seen in Figure 42(b). These stringers were observed to be either 90 ˚, inclined or along the tensile axis direction in investigated specimens.

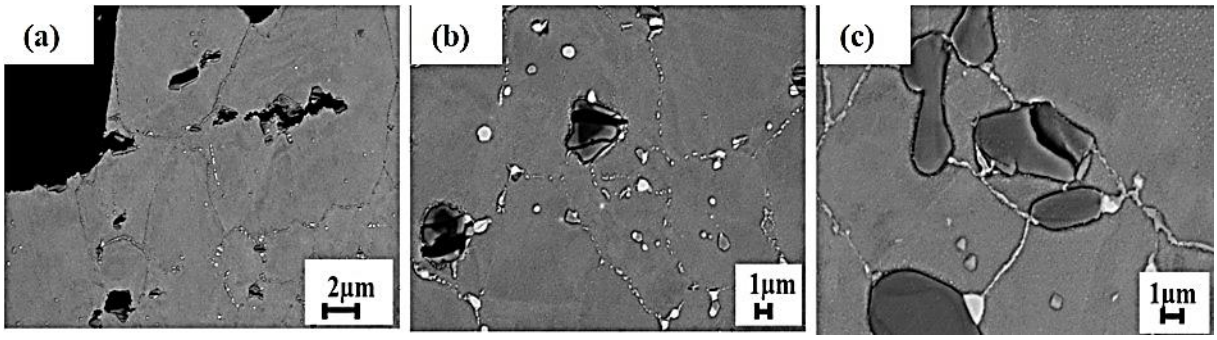

Figure 42 A longitudinal section of fractured specimen showing (a) Cracks in carbides just below the fracture surface (b) Segregation of carbides within a band of carbide stringer (c) MC carbides as large as the smaller grains. Presence of a crack in MC carbide at grain boundary

Figure 42 (c) shows carbides of a size almost similar to the size of smaller grains. As shown in Figure 43, γ′ precipitates are seen to be distributed uniformly in a matrix. Figure 43(a) shows the presence of a bimodal distribution of coarse, intragranular and fine γ′ near to grain boundaries. It also shows the presence of cracked MC carbide at the grain boundary. However, in one of the conventionally heat-treated forgings, γ′ is uniformly distributed in size and shape intragranularly and near grain boundaries, as seen in Figure 43(b).

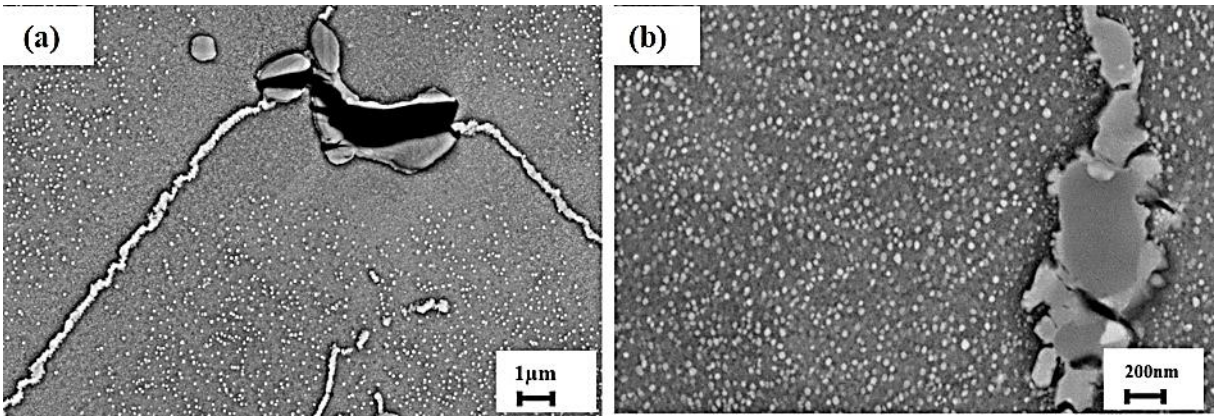

Figure 43 . SEM image showing (a) Uniform distribution of spherical γ' and crack in MC carbide at the grain boundary in forging (heat-treated according to AMS 5951) (b) Distribution of very fine γ' near grain boundary and intragranularly (conventional heat treatment).

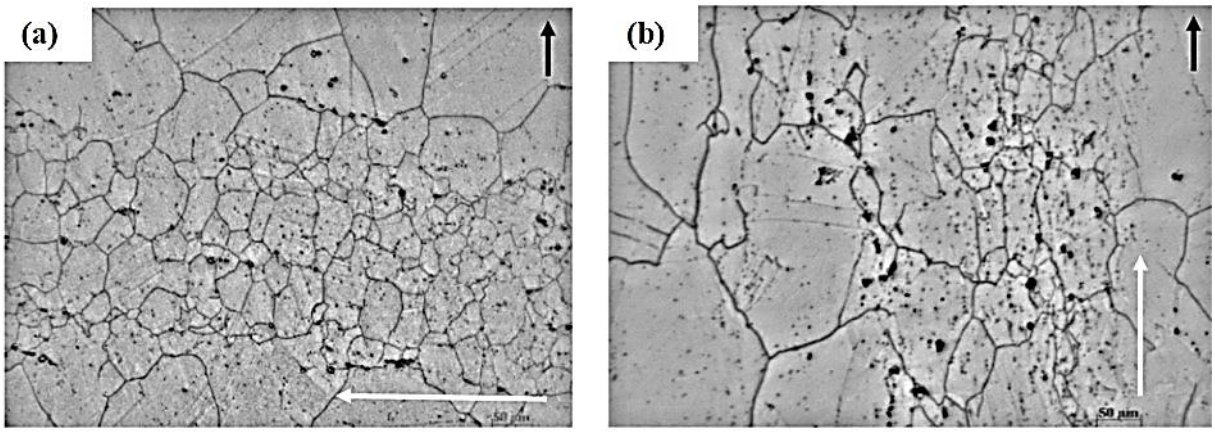

Figure 44 Optical microscopic images showing carbide stringer and bimodal distribution of grains in specimens from short transversal (ST) direction (a) Specimen with 12 % elongation: showing carbides perpendicular (white arrow) to tensile axis direction (black arrow) (b) Specimen with 16 % elongation: showing carbides along (white arrow) the tensile axis direction (black arrow)

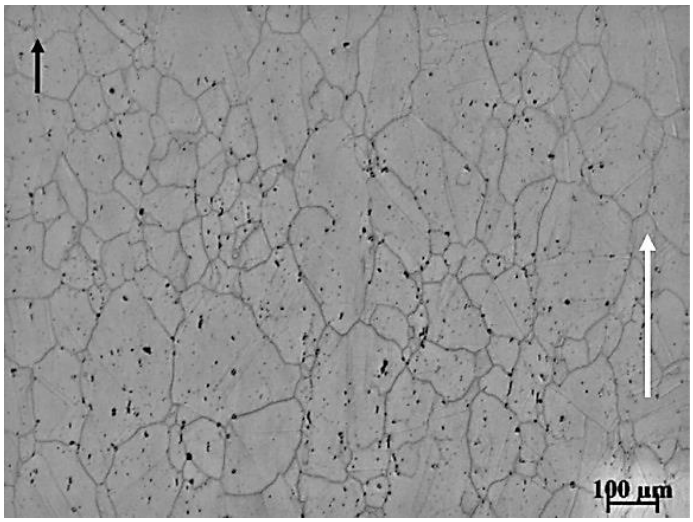

Figure 45 Optical microscopic images showing the carbide stringer and bimodal distribution of grains in specimens from LT direction with 24 % elongation: showing carbides uniformly distributed in the matrix along the tensile axis direction (black arrow)

The optical microscopy of the specimens shows the presence of smaller grains in regions where carbide segregations are observed, while regions outside of carbide segregation are coarse grains, as seen in Figure 44. Figure 44(a) is an optical image of a specimen from ST direction from forging, which measured ductility at 12 %. The carbide distribution was seen 90 ˚ to the tensile axis (black). In Figure 44(b) a specimen with 16 % elongation showed the presence of carbide stringers along the tensile axis direction, while specimens from LT direction had uniformly distributed carbides along the tensile axis direction, as seen in Figure 45.

Chapter 6

Conclusions

The major findings and conclusions from this work are summarized as follows,

- The precipitation of γ′ in Haynes 282 is rapid enough to ocurr during air cooling of sheet material from the homogenisation treatment. As a result, nano-scale precipitates were found in the MA condition. However, on rapid quenching γ′ precipitation during cooling is suppressed.
- The coarsening kinetics of the γ′ particles corresponds to the LSW theory, and no morphological changes are observed even for longer ageing times of 98 h between 650 °C and 800 ºC.
- The morphology of grain boundary carbides depends strongly on temperature. With increasing ageing temperature, the morphology changes from continuous film, to brick wall structure and finally to discrete particles. However, no further morphological changes were observed with increasing ageing time.
- The experimentally determined solvus temperature of the hardening phase, γ′, was determined at just above 1010 °C, higher than the 997 °C previously suggested in literature.
- The variations of the solution treatment temperature and cooling rate studied here shows that grain boundary carbides remain undissolved at the extreme of currently permitted specification limits on solution temperatures, but there is no impact on the microstructure and properties after full ageing. The γ′ morphology and size is not affected after full ageing despite a variation in the initial solution treatment conditions.
- The solution treatment parameter variation does not affect the strength of the material but influences the ductility to some extent. Direct ageing from mill-annealed state showed similar behaviour, as is the case with additional solutionising.
- The variations of the carbide stabilisation temperature and cooling rate studied here do not have any significant effect on the morphology of the grain boundary carbides, but drastically alter the size, morphology and distribution of γ’ after subsequent ageing at 788 °C. Excluding the carbide stabilisation step, had no noticeable impact on the γ’ structure but produced more continuous interconnected grain boundary carbides.
- Variations in carbide stabilisation treatment had some impact on the strength levels, ductility and work hardening.
- Anisotropic ductility in the case of forgings is primarily due presence and orientation of carbide stringers. The formation of carbide stringers during forging and subsequent heat

treatment is due to local elemental segregation in the ingot. As the MC and M_6C carbides are brittle, cracks are initiated and propagated under loading conditions. These carbide stringers pin the grain boundaries and result in bimodal grain size distribution. The preferential alignment of carbide stringers and bimodal distribution is microstructural inhomogeneity, which influences the measured tensile ductility. Ductility is thus anisotropic and inhomogeneous, which has been qualitatively confirmed in the modelling attempt, where the orientation of carbides at an angle of 45 ˚ to the tensile axis shows maximum ductility compared to those at an angle of 90˚.

Recommendations for future work

The work within this project was mainly carried out in order to understand the microstructural development in Haynes 282 sheet material, which had a uniform grain size distribution and to correlate these changes to the tensile properties at different temperature conditions. There are many aspects that are still not covered in this study. Some of the suggestions are

1. To investigate how the microstructural changes in terms of γ′ and carbide morphology can affect the fatigue and creep properties of the material.
2. To investigate how the effects of local chemical segregations, and grain size variations as seen in the case of forgings can also translate to changes in microstructure on heat treatment.
3. To investigate further why high temperature solutionising at 1120 ºC for 2 h introduced grain growth and also changed the γ′ morphology during subsequent ageing steps.

References

[1] L. Pike, *Development of a fabricable gamma-prime strengthened superalloy*, Proceedings of the International Symposium on Superalloys, (2008) pp. 191-200

[2] Roger C Reed, *The Superalloys Fundamentals and Applications*, Cambridge University Press, (2008).

[3] R.F.Smith et.al., *Development and application of nickel alloys in aerospace engineering*, Aircraft engineering and aerospace technology, Vol 73, Issue 2 (2001) pp. 138-146

[4] T.M.Pollock, *Nickel-based superalloys for advanced turbine engines: Chemistry, microstructure and properties*, Journal of Propulsion and power, Vol22, No2 (2006) pp. 361-374

[5] R.N.Ghosh, *Superalloy:Processing and performance*, Report (National metallurgical laboratory, India), pp. 97-106

[6] C.T.Sims, *A contemporary view of Ni-based superalloys*, Journal of Metals (1966) pp. 1119-1130

[7] J.Chander, *The hardening mechanism and corrosion resistance of nickel-base alloys A review*, Canadian Metallurgical Quarterly, Vol 3, No.1 (1964) pp. 57-77

[8] J.C.Zhao et.al., *The thermodynamic prediction of Phase stability in multicomponent superalloys*, Journal of metals (2002) pp. 37-41

[9] M.Kaufman et.al., *The Phase structure of Inconel 718 and 802 alloys*, Transactions of the metallurgical society of AIME, Vol 221 (1961) pp. 1253-62

[10] C.H.Lund et.al., *Identification of Microconstituents present in superalloys*, Defense metals information center (1962) pp. 1-22

[11] G.P.Sabol et.al., *Microstructure of Nickel based superalloys*, Phys. Stat.Sol. 35, 11 (1969), pp. 11-52

[12] P.S.Kotval, *The microstructure of Superalloys*, Metallography, 1 (1969) pp. 251-285

[13] L. Pike, *Haynes 282alloy - a new wrought superalloy designed for improved creep strength and fabricability*, Proceedings of the ASME Turbo Expo 4 (2006) pp. 1031-1039.

[14] D.R.Muzyka, *Controlling microstructures and properties of superalloys via use of precipitated phases*, Metals engineering quarterly (1971) pp. 12-19

[15] D.L.Kalstrom et.al., *Structure property relationship in solid solution strengthened superalloys*, Superalloys (1984) pp. 553-562

[16] A.R.P.Singh et.al., *Influence of cooling rate on the development of multiple generations of γ' precipitates in a commercial nickel-base superalloy*, Materials characterization ,Vol 62 (2011) pp. 878-886

[17] J.R.Mihalisin et.al., *Microstructural study of the response of a complex superalloy to heat treatment*, Transactions of the metallurgical society of AIME, Vol 215 (1959) pp. 912-916

[18] H.J.Murphy et.al., *Long time structures and properties of Three high strength, nickel-base alloys*, Transactions of the metallurgical society of AIME, Vol 239 (1978) pp. 1961-67

[19] W.Betteridge et.al., *The effect of heat-treatment and structure on the creep and stress-rupture properties of Nimonic 80A*, Journal of the Institute of metals, Vol 85, 1956, pp. 473-479

[20] E.Balikci et.al., *Influence of various heat treatments on the microstructure of polycrystalline IN738LC*, Metallurgical and Materials Transactions A , Vol 28A (1996) pp. 1993-2003

[21] A.Wisniewski et.al., *Influence of grain-boundary morphology on creep of a wrought Ni-base superalloy*, Materials science of Engineering A , 510-511 (2009) pp. 266-272

[22] J.Radavich et.al., *Effect of processing and composition on the structure and properties of P/M EP741NP Type Alloys*, Chinese Journal of Aeronautics, 20 (2007) pp. 097-106

[23] G.Bai et.al., *Effect of temperature on tensile behavior of Ni-Cr-W-based superalloy*, Materials science and engineering A, 528 (2011) pp. 1974-1978

[24] Z.W.Lian et.al., *Temperature dependence of tensile behavior of Ni-based superalloy M951*, Materials science and engineering A, 489 (2008) pp. 227-233

[25] X.G.Wang et.al., *Tensile behaviors and deformation mechanisms of a nickel-base single crystal superalloy at different temperatures*, Materials Science and Engineering A, (2013) pp. 1-21

[26] P.R.S.A e Silva et.al., *Solution heat-treatment of Nb-modified MAR-M247 superalloy*, Materials characterization, 75 (2013) pp. 214-219

[27] J.Li et.al., *Effect of heat treatment on microstructure and mechanical properties of laser melting deposited Ni-base superalloy Rene 41*, Materials science and engineering A, 550 (2012) pp. 97-102

[28] W.P.Danei, et.al., *Phase reaction s in B-1900 Nickel-Base alloy from 1600 to 1800 F*, Transactions of American society of metals, Vol 59 (1966) pp. 505-516.

[29] F.Torster et.al., *Influence of grain size and heat treatment on the microstructure and mechanical properties of the nickel-base superalloy U720 LI*, Materials science and engineering A234-236 (1997), pp. 189-192

[30] E.G.Richards, *Factors influencing the stability of nickel-base high temperature alloys*, pp. 1-23

[31] J.F.Radavich et.al., *A study of phase reactions in a complex 4.5Al-3.5Ti –Ni Base alloy*, Advances in X-Ray Analysis (1961) pp. 233-245

[32] H.E.Collins, *Relative stability of carbide and intermetallic phases in nickel-base superalloys* (1968) pp. 171-198

[33] H.E.Collins et.al., *Carbide and intermetallic Instability in Advanced Nickel-Base Superalloys*, Transactions of the ASM, Vol 61(1968) pp. 139-148

[34] R.M.Kearsery et.al., *Microstructural effects on the mechanical properties of ATI718Plus Alloy*, Journal of Metals, 64, (2012) pp. 241-251

[35] X.Dong et.al., *Microstructure of carbides at grain boundaries in nickel-based superalloys*, Journal of Material science and Technology A, 28(11) (2012) pp. 1031-1038

[36] Y.Feng Shi et.al, *Effect of melt superheating on the morphology of MC carbide in a Cast Ni-base Superalloy M963*, Journal of Wuhan University of Technology, 17(3), (2002) pp. 42-45

[37] C.P.Sullivan et.al., *Some effects of microstructure on the mechanical properties of nickel-base superalloys*, National metal congress (1966) pp. 1-29

[38] S.Fox et.al., *Influence of carbides on the mechanical properties on Inconel 718*, Proceedings of the 7th International Conference on the Strength of Metals and Alloys, Montreal, Canada, Vol 1, 12–16 August (1985) pp. 399-404

[39] L.Liu et.al, *Effect of solidification conditions on MC carbides in a nickel-base superalloy IN738LC*, Scripta Metallurgica et Materialia, 30 (1994) pp. 587-591

[40] J.Yang, et.al., *Relative stability of carbides and their effects on the properties of K465 superalloy*, Materials science and engineering A, 429 (2006) pp. 341-347

[41] J.M.Larson, *Carbide morphology in P/M IN 792*, Metallurgical transactions A, Vol 7A, (1976) pp. 1497-1502

[42] J.Chen et.al., *MC carbide formation in directionally solidified MAR-M247 LC superalloy*, Materials science and engineering A, 247 (1998) pp. 113-125

[43] X.Z.Qin et.al., *Decomposition of primary MC carbide and its effect on the fracture behaviors of a cast Ni-base superalloy*, Material science and Engineering A, 485 (2008) pp. 74-79

[44] B.G.Choi et.al., *Temperature dependence of MC decomposition behavior in Ni-Base superalloy GTD 111*, Materials science and Engineering A, 478 (2008) pp. 329-335.

[45] G.Bai et.al., *Effect of thermal exposure on the stability of carbides in Ni-Cr-W based superalloy*, Materials Science and Engineering A ,528 (2011) pp. 2339-2344

[46] L.Jiang, et al., *The effect of M23C6 carbides on the formation of grain boundary serrations in a wrought Ni-based superalloy*, Materials Science and Engineering A, 536 (2011) pp. 37-44

[47] R.Hu et al., *Precipitation behavior of grain boundary M23C6 and its effect on tensile properties of Ni-Cr-W based superalloy*, Materials Science and Engineering A, 548 (2012) pp. 83-88

[48] A.J.Wasson et al., *The effect of carbide morphologies on elevated temperature tensile and fatigue behavior of a modified single crystal Ni-Base superalloy*, Proceeding at conference ,Superalloy (2008) pp. 489-497

[49] Yu.Zhu-huan et al., *Effect of solidification rate on MC type carbide morphology in single crystal Ni-base superalloy AM3*, Trans.Nonferrous Met. Soc.China , 20 (2010) pp. 1835-1840

[50] Q.Z.Chen, *Effect of alloying chemistry on MC carbide morphology in modified RR2072 and RR2086 SX superalloys*, Scripta Materialia, 47 (2002) pp. 669-675

[51] A.R.P.Singh et al, *Mechanisms related to different generations of γ′ precipitation during continuous cooling of a nickel-base superalloy*, Acta Materialia, 61 (2013) pp. 280-293

[52] S.Zhao et al., *Gamma prime coarsening and age-hardening behaviors in a new nickel base superalloy*, Materials Letters, 58 (2004) pp. 1784-1787

[53] A.M.Ges et al., *Coarsening behavior of a Ni-base superalloy under different heat treatment conditions*, Materials science and engineering A, 458 (2007) pp. 96-100

[54] J.Tiley, *Coarsening kinetics of γ′ precipitates in the commercial nickel-base superalloys Rene 88DT*, Acta Materialia, 57 (2009) pp. 2538-2549

[55] K A Heck, *The Time-Temperature-Transformation behavior of Alloy 706, Superalloys*

[56] X.Xie et al., *TTT diagram of a newly developed nickel-base superalloy - ALLVAC 718 Plus,* Superalloys 718, 25, 706 and derivatives 2005, TMS (2005), pp. 193-201

[57] A.O.Basile et.al, *A current TTT diagram for wrought alloy 718*, Superalloys 718, 25, 706 and derivatives, pp. 325-335

[58] S.Mannan et.al, *Time-Temperature transformation diagram of Alloy 725*, Superalloys 718, 625,706 and various derivatives, pp. 345-356

[59] J.C.Zao, et al., *Phase precipitation and time-temperature-transformation diagram of Hastealloy X*, Materials Science and Engineering A, 293, (2000), pp. 112-119

[60] P.Ganesan et al., *Development of a Time-Temperature Transformation diagram for Alloy 925* , Corrosion Vol44, 11,(1988) pp. 827-835

[61] L.Ferrer et al., *Microstructural evolution during thermomechnical processing of alloy 625*, Superalloys 718, 625, 706 and various derivatives, pp. 217-227

[62] Mannan et al., *Time-Temperature-transformation diagram of Alloy 945*, 7th International symposium on Superalloys 718 and derivatives, pp. 629-643

[63] H.White et al., Weldability of Haynes 282, *Alloy for new fabrications and after service exposure*. , Energy Materials, Volume 4,2009, pp. 84-91

[64] http://www.haynesintl.com/pdf/h3173.pdf

[65] C.J.Boehlert et al., *A comparison of the microstructure and creep behavior of cold rolled Haynes 230 alloy and Haynes 282 alloy*, Materials science and engineering A, 528 (2011), pp. 4888-4898.

[66] Natalia Sobczak et al., *Castability of Haynes 282 alloy, Workshop "Advanced Ultrasupercritical Coal-fired Power Plants*", EVN Forum Maria Enzerdorf Vienna, Austria, 19-20 September (2012)

[67] Hubert Matysiak et al. , *Microstructure of Haynes 282 Superalloy after Vacuum Induction Melting and Investment Casting of Thin-Walled Components, Materials* (2013) 6, pp. 5016-5037

[68] P D. Jablonski et al., *Processing of Advanced Cast Alloys for A-USC Steam Turbine Applications*, JOM, Vol. 64, No. 2, (2012)

[69] J.J.Sobczak et al., *Numerical analysis of the casting process of Haynes 282 alloy* , Advanced sustainable foundry 19-21 May (2014)

[70] Y.Yang et al., *Microstructural evolution in cast Haynes 282 for application in advanced power plants* , 7th International Conference on Advanced in Materials Technology for Fossil Power Plants, At Waikola, Hawaii USA, Volume: 1

[71] L.O.Osoba et al., *Improved resistance to laser weld heat-affected zone microfissuring in a newly developed superalloy Haynes 282*, Metallurgical and Materials transactions A 43A, Nov (2012) pp. 4281-4296

[72] L.O.Osoba et al., *Cracking Susceptibility After Post-Weld Heat Treatment in Haynes 282 Nickel-Based Superalloy*, Acta Metall. Sin. (Engl. Lett.) Vol.26 No. 6 pp. 747—753 December (2013)

[73] Jeremy Carona et al., *Weldability of HAYNES 282 superalloy after long-term thermal Exposure* MATEC Web of Conferences 14, 13003 (2014)

[74] R.A.Buckson et al., *Analysis of the Influence of Laser Welding on Fatigue Crack Growth Behavior in a Newly Developed Nickel-Base Superalloy*, Journal of Materials Engineering and Performance

[75] J.Jacobsson et al., *Weldability of Ni-Based Superalloys Waspaloy® and Haynes 282- A Study Performed with Varestraint Testing* , Research & Reviews: Journal of Material Sciences 4 (2016)

[76] F.Hanning et al., *Weldability of wrought Haynes 282 repair welded using manual gas tungsten arc welding* Research paper Weld World August (2017)

[77] Joel Andersson et al., *Hot Ductility Study of HAYNES 282 Superalloy*, Proceeding of the 7th International Symposium on Superalloy 718 and Derivatives, TMS , pp. 539-554

[78] D. A. Metzler, A *Gleeble®-based Method for Ranking the Strain-Age Cracking Susceptibility of Ni-Based Superalloys*, Welding Journal Oct (2008) Vol 87, pp. 249-256.

[79] L.O.Osoba, *Study on Laser weldability improvement of newly developed Haynes 282 superalloy* PhD thesis (2012).

[80] C.J. Boehlert et al., *A comparison of the microstructure and creep behavior of cold rolled HAYNES 230 alloy and HAYNES 282 alloy*, Materials Science and Engineering A, 528 (2011) pp. 4888–4898.

[81] P.F. Tortorelli et al., *Creep rupture behavior of precipitation strengthened Ni-Based alloys under advanced ultrasupercritical steam conditions.*

[82] D.H.Bechetti et al., *Microstructural Evolution and Creep-Rupture Behavior of A-USC Alloy Fusion Welds,* et al. Metallurgical and Materials Transactions A, 4502, Vol 47 A, Sept (2016).

[83] L.M:Pike, *Low cycle fatigue behavior of Haynes 282 Alloy and other wrought gamma prime strengthened alloys*, Haynes International, Kokomo, IN 46904-9013 Proceedings of GT2007, ASME Turbo Expo 2007: Power for Land, Sea and Air, May 14-17, (2007) Montreal, Canada

[84] R.A. Buckson et al., *Cyclic deformation characteristics and fatigue crack growth behaviour of a newly developed aerospace superalloy Haynes 282 ,* Materials Science and Engineering A, 555 (2012) pp. 63– 70

[85] Kyle A. Rozman , *Characterization of High Temperature Fatigue Mechanisms in Haynes 282 Nickel-Based Superalloy* PhD thesis

[86] K. Barat et al., *Ultrasonic quantification of high temperature cyclic damage in an advanced nickel-based superalloy,* Materials Science and Engineering A, Nov (2014)

[87] J. He et al. Low-Cycle *Fatigue Properties of a Nickel-Based Superalloy Haynes 282 for Heavy Components*. Journal of Materials Engineering and Performance Volume 26(5) May (2017)—2257

[88] L. M. Pike and S.K. Srivastava, "*Oxidation Behavior of Wrought Gamma-Prime Strengthened Alloys*", Materials Science Forum, Vols. 595-598, (2008) pp. 661-671

[89] M Bruchhausen, et al., *Impact of High Pressure Hydrogen Atmosphere on the Mechanical Properties of Haynes 282* Superalloy. Materials Testing: Vol. 54, No. 9, (2012), pp. 612-618.

[90] P.D.Jablonski et al., *Effects of Al and Ti on Haynes 282 with fixed gamma prime content*, 7th International symposium on Superalloy 718 and Derivatives, pp. 617-628.¨

[91] S.Haas et al., *Correlation of precipitate evolution with Vickers hardness in Haynes 282 superalloy: In-situ high-energy SAXS/WAXS investigation* Materials Science & Engineering A, 711 (2018) pp. 250–258

[92] C.Joseph et al., *Influence of heat treatment on the microstructure and tensile properties of Ni-base superalloy Haynes 282*, Materials Science and Engineering A, 679 (2017), pp. 520-530.

[93] Z.H.Zhong et al., Tensile *Properties and Deformation Characteristics of a Ni-Fe-Base Superalloy for Steam Boiler Applications*, Metall. Mater. Trans. A, 45 (2014), pp. 343-350

[94] H.F. Sun et al., *Microstructure heterogeneity and creep damage of DZ125 nickel-based superalloy*, Prog. Nat. Sci.: Mater. Int., 24 (2014), pp. 266-273

[95] X.Zhao, *Effect of heat treatment on the microstructure of a Ni–Fe based superalloy for advanced ultra-supercritical power plant applications***,** Prog. Nat. Sci.: Mater. Int., 26 (2014), pp. 204-209

[96] ASTM E8, Standard Test Methods for Tension Tests of Metallic Materials.

[97] ASTM E21, Standard Test Methods for Elevated Temperature Tension Tests of Metallic Materials, 2009

[98] ASTM E92, Standard Test Methods for Vickers Hardness and Knoop Hardness of Metallic Materials

[99] A.M.Ges et al., *Coarsening behaviour or a Ni-base superalloy under different heat treatment conditions*, Mater. Sci. Eng. A, 458 (2007) pp. 96-100

[100] A.Baldan, *Review Progress in Ostwald ripening theories and their applications to nickel-base superalloys-Part 1: Ostwald ripening theories,* J.Mater. Sci. 37 (2002) pp. 1971-2202

[101] I.M.Lifshitz , *The kinetics of precipitation from supersaturated solid solutions,* J.Phys.Chem.Solids 19 (1961), pp. 35-50

[102] C.Wagner, *Theory of precipitate change by redissolution*, Z. Elektrochem, 65, (1961), pp. 581-591

[103] David Porter, "Phase transformation in metals", Third edition, Taylor & Francis Group 2008.

[104] D. U. Furrer et.al., *Microstructure and mechanical property development in superalloy U720LI*," Superalloys 2000, pp. 415-424.

Acknowledgements

Firstly I would like to thank, My Parents for their love, care and support to me and my little ones (Adina and Alina) for the past year. Their sacrifice and inconveniences during this period is appreciated and unforgettable. An impossible journey was possible with having you both onboard! Dad and Mom, you both are my strength and my support.I owe my deepest gratitude to my husband Anoop Thomas for always being a source of help, support and encouragement in all my pursuits. I love you all!

I would like to heartily thank my advisor Professor Christer Persson for his continued encouragement and patience during this project for all these years. (We managed to finish this project without doing any rituals in our testing lab. Yipeee!!!!)

My sincere thanks goes to my co-supervisor Dr. Magnus H Colliander who believed that I could still do a good work in spite of all the troubles that we faced. His continued encouragement, critical comments and stimulus questions and timely response in critical situations helped me get out of the situation very peacefully. I am really very grateful for your mentorship and enjoyed working with you. You have all what it needs to be in a good supervisor .You truly deserve the best!

GKN aerospace introduced me to the world of superalloys and Haynes 282. I'd like to gratefully acknowledge members of the GKN Aerospace in Sweden, who has been directly and indirectly involved within this project for all their support and input. Special thanks to Bengt Pettersson who helped me chase everyone in the industry during all these years for both technical and non-technical support. Frank Skystedt, Johan Tholerus and Joel Andersson for their inputs and discussion on Haynes 282. Thanks to Rebecka Brommesson, my twin PhD within the NFFP 6 program and colleague, we have had really good discussion both within and outside the scope of this research work. I always enjoyed it. .

My fellow colleagues at the department was indeed a good source of advice and collaboration and a friendly work environment both in teaching and research.

Special thanks to Kenneth Hamberg (Etching ☹) , Eric Tam, Roger Sagdahl (my laptop was never friendly to me but always to him☺), Gustav Holmqvist , Yiming Yao, Peter Sotkovsky,

Håkan Millqvist (He was my astronaut for Quenching experiments ☺) for their help with technical issues and with experimental techniques which was indeed a great support for the completion of my thesis.

My friends Ajay-Trupti, Zubair-Rashmi, Aditi, Shodix – Stella, for all their support and encouragement, and to keep me motivated every now and then. Thank you for your love and belief in me!

Last but not the least *Thanking GOD Almighty* for all the strength and courage that I have had to face the situations on a positive note.

This acknowledgement is incomplete without a thankful note to Migrationsverket! Thank you! I have had all the pleasure to interact with them several times during the past 1 year. I learned a lot to deal with Migrationsverket but at my cost☹ !!!!!

“Keep **Smiling** and One day Life will get tired of upsetting you”- Unknown

“It’s **impossible**”, said pride,

“It’s **risky**”, said experience,

“It’s **pointless**”, said reason,

“Give it a **try**”, whispered the **heart** – Unknown

“Don’t give up. Normally it is the **Last key** on the Ring which **Opens** the Door” – Paulo Coelho